UNIVERSITY *of* York

This is a repository copy of *Synthesis, Mesomorphism, and Photophysics of 2,5-Bis(dodecyloxyphenyl)pyridine Complexes of Platinum(IV)*.

White Rose Research Online URL for this paper:
https://eprints.whiterose.ac.uk/id/eprint/138756/

Version: Accepted Version

White Rose
university consortium
Universities of Leeds, Sheffield & York

eprints@whiterose.ac.uk
https://eprints.whiterose.ac.uk/

Synthesis, Mesomorphism and Photophysics of 2,5-Bis(dodecyloxyphenyl)pyridine Complexes of Platinum(IV)[§]

Rachel R. Parker, Julia P. Sarju, Adrian C. Whitwood,

J. A. Gareth Williams[†], Jason M. Lynam* and Duncan W. Bruce*

Department of Chemistry
University of York
Heslington
YORK
YO10 5DD
UK
Tel: (+44) 1904 324085
E-mail: duncan.bruce@york.ac.uk; jason.lynam@york.ac.uk

[†] Department of Chemistry
Durham University
University Science Laboratories
South Road
DURHAM
DH1 3LE
UK

[§] Dedicated with much affection to Peter Maitlis on the occasion of his 85th birthday.

Abstract:

It has been shown for the first time that the Pt^{IV} complex *cis*-[Pt(N^C-tolpy)$_2$Cl$_2$] (tolpy = 2-(4-tolyl)pyridinyl) can be prepared in a one-pot reaction from K$_2$[PtCl$_4$], although analogous complexes containing 2,5-bis(4-dodecyloxyphenyl)pyridine (=HL) could be prepared using existing routes. The resulting complexes *cis*-[Pt(N^C-L)$_2$Cl$_2$] are liquid crystals and small-angle X-ray scattering suggests formation of a lamellar mesophase. Surprisingly, heating [Pt(κ^2-N^C-L)$_2$X(κ^1-N^C-LH)] also leads to a mesomorphic compound, which results from thermally induced oxidation to *cis*-[Pt(N^C-L)$_2$Cl$_2$] and what is presumed another geometric isomer of the same formula. The Pt^{IV} complexes are quite strongly luminescent in deoxygenated solution, with $\phi \approx 10\%$ and show vibrationally structured emission spectra, $\lambda_{max}(0,0)$ = 532 nm, strongly displaced to the red compared to *cis*-[Pt(N^C-tolpy)Cl$_2$]. Long luminescence lifetimes of 230 μs are attributed to a lower degree of metal character in the excited state accompanying the extension of conjugation in the ligand. There is no significant difference between the emission properties of the bromo- and chloro-complexes, in contrast with the known complexes *cis*-[Pt(N^C-ppy)X$_2$], where the quantum yield for X = Br is some 30 times lower than for X = Cl (ppyH = 2-phenylpyridine). The lower energy of the excited state in the new complexes probably ensures that deactivating LLCT/LMCT states remain thermally inaccessible, even when X = Br.

Introduction

Research into luminescent complexes of heavy transition metals has been of great interest in recent years due to the potential application of such systems in multidisciplinary research areas and technologies. In particular, intense interest has been shown in the incorporation of such complexes in OLED devices, as well as wide applications in other materials such as photovoltaic devices, solar cells and thin film transistors (TFTs).[1] In some complexes of heavy transition metals, the spin selection rules of the systems is modified owing to the large degree of spin-orbit coupling, which allows ready radiative decay from the triplet manifold, increasing the theoretical maximum efficiency of emission.[2] It is this that has allowed the commercial exploitation of complexes of six-coordinate iridium(III).[3]

Among the other metal-based chromophores that have been studied, d^8 systems based on gold(III)[4] and platinum(II)[5] have attracted a good deal of interest, but more recently there is published work that concentrates on six-coordinate platinum(IV). Utilising bidentate cyclometallating ligands such as 2-phenylpyridine (ppy), platinum(IV) complexes have been obtained that show high-energy, long-lasting phosphorescence.[6]

The first instance of platinum(IV) complexes emitting at room temperature was reported by Chassot *et al.* in the mid-1980s, with complexes based on functionalised ppy and 2-(2-thienyl)pyridine) (Figure 1a).[7] Since then, families of platinum(IV) complexes based on functionalised cyclometallating ligands have been published. Jenkins and Bernhard reported a library of cationic platinum(IV) complexes based on the $[Pt(C{\wedge}N)_2(N{\wedge}N)]^+$ structure, where C^N are functionalised 2-phenylpyridine ligands and N^N are functionalised 2,2'-bipyridines (Figure 1b).[8] More recently, Juliá *et al.* have reported a series of tris(cyclometallated)platinum(IV) complexes, which differ in emissive properties between isomers (Figure 1c),[6b] as well as numerous reports into the influences of functionalising the cyclometallating ligands and altering the ancillary ligands in the system (Figure 1d and e).[6a, 9]
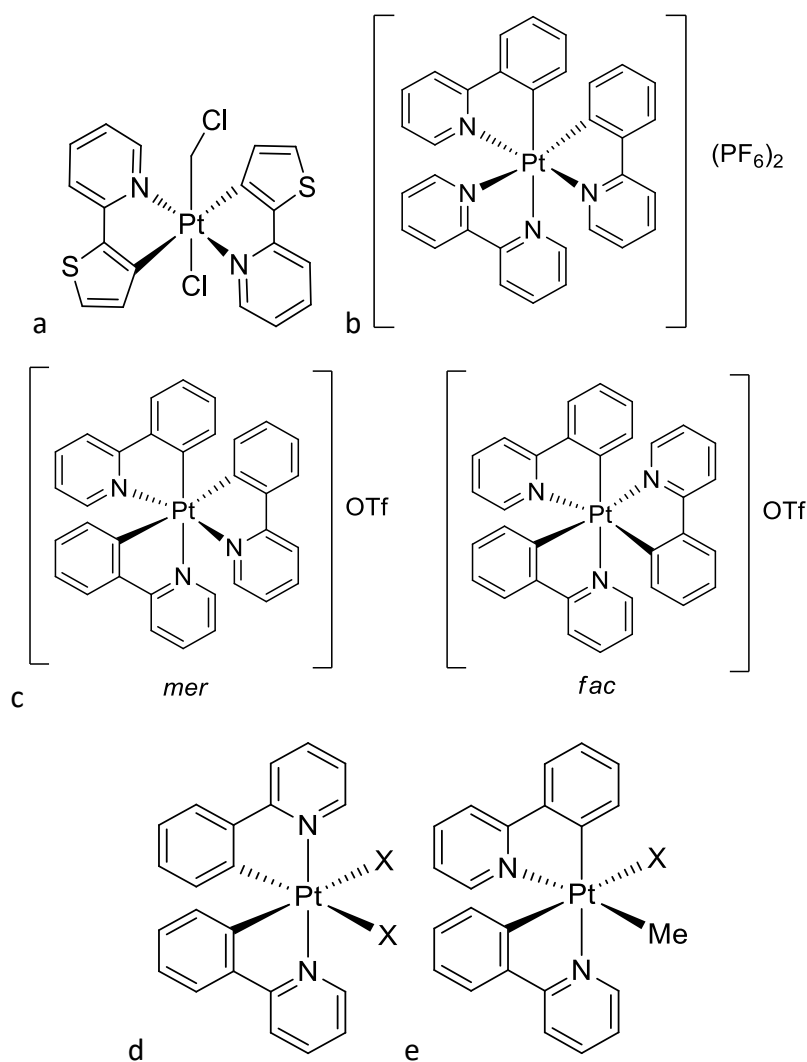
Figure 1: Model structures from a) Chassot *et al.*[7] who reported a platinum(IV) system with 2-(2-thienyl)pyridine) ligands after the oxidative addition of CH_2Cl_2; b) Jenkins and Bernhard[8] showing the [Pt(C^N)$_2$(N^N)]$^+$ base unit, with reported functionalisation of both the C^N and N^N rings with fluorine and methoxy groups; c) the *mer* and *fac* isomers of the base unit of tris(cyclometallated)platinum(IV) complexes reported by Juliá *et al.*[6b], with reported functionalisation of the C^N rings with fluorine and methyl groups, as well as systems where the pyridyl ring is replaced with pyrazole; Juliá *et al.*[9a] showing d) symmetric and e) asymmetric bis-cyclometallated 2-phenylpyridine systems, where X = F, Cl, Br, I, OTf, OAc, TFA.

One interesting modification of emissive metal complexes is to tune the molecular structure to induce liquid-crystalline properties. The long-range order inherent in liquid crystal mesophases can facilitate greater charge-carrier mobilities (leading to lower drive voltages), while aligned systems can lead to polarised emission.[10]

However, while liquid-crystalline derivatives of square-planar platinum(II) are ubiquitous, including those with emissive properties, liquid crystals based on platinum(IV) present a different

challenge. The molecular anisotropy associated with liquid crystals is not readily achieved with octahedral or pseudo-octahedral (*e.g.* D_3 or C_2 symmetry) metal centres and there remain relatively few examples of metallomesogens based on six-coordinate metals.[11],[12] Mesomorphic platinum(IV) systems in particular are extremely rare in the established literature. Work by Ghedini *et al.* developed liquid-crystalline platinum(IV) systems, formed from the oxidative addition of I_2 or MeI to platinum(II) precursors containing cyclometallated azobenzenes and β-diketonates.[13] As might have been expected for systems with a reduced ability to organise side-by-side, the liquid crystal behaviour was dominated by the formation of nematic phases, often at quite elevated temperatures. There is also an isolated report of some platinum(IV) complexes based on 4,4'-disubstituted bipyridines bound to a $PtCl_4$ unit, but the mesophases are not well characterised, with the SAXS patterns showing more order than might normally be associated with liquid-crystalline phases.[14]

However, we and others[5f, 10e, 15] have reported a series of six-coordinate iridium(III) complexes that show liquid-crystalline properties. The examples from our own work, shown in Figure 2, show columnar mesophases, which is remarkable considering the low level of ligand functionalisation, *i.e.* only two chains per ligand.[5f] This led to speculation that the structurally analogous complexes of platinum(IV) might be prepared, which could combine emission and liquid-crystalline behaviour.
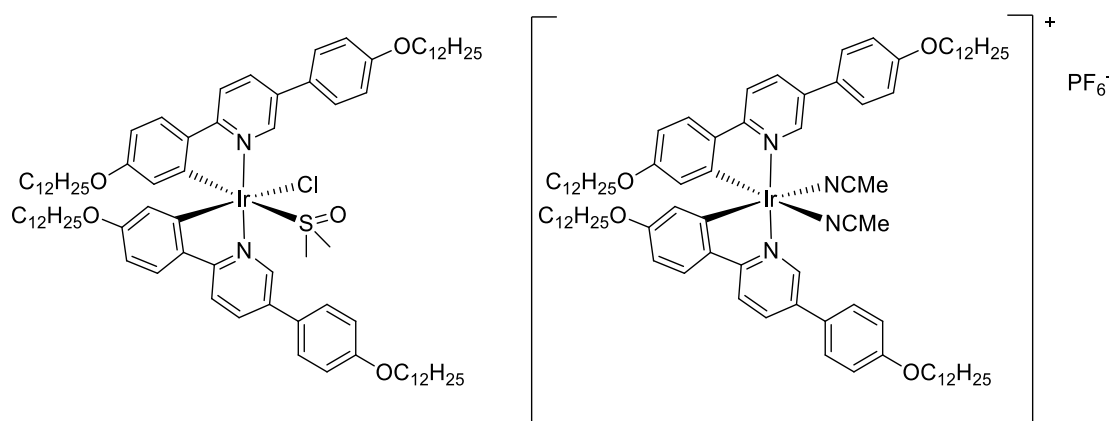

Figure 2: Liquid-crystalline complexes of Ir(III) previously synthesised by our group[5f]

Results

Synthesis

The target complex contains a platinum with two *cis*-coordinated, *ortho*-metallated ppy derivatives and two monodentate chloride ligands in mutually *cis* positions. There is a direct analogy with the iridium(III) chemistry, but in that case of +3 metal centre, the complexes feature one anionic chloride with the sixth site occupied by a neutral ligand. The parent Pt^{IV} compound, based on ppy, has been prepared previously as shown in Scheme 1, in which the platinum(II) precursor [Pt(N^C-ppy)Cl(N-ppyH)] was oxidised by an iodine(III) reagent or peroxide with a concomitant second C–H activation.[6, 8-9, 16] However, following our earlier observation of the formation of dinuclear platinum(III) complexes *via* oxidation of platinum(II) precursors using dmso/H$^+$,[17] we had been investigating the synthesis of related complexes under different conditions. We found that it is possible to prepare the colourless Pt^{IV} complex [Pt(tolpy)$_2$Cl$_2$] **1** directly, in 34% isolated yield, from K$_2$[PtCl$_4$] and 2-tolylpyridine (tolpyH) on heating in 2-ethoxyethanol in the presence of dmso (route B in Scheme 1). Single crystals were obtained and details of the structure are given below. The reaction could also be carried out under microwave irradiation at ambient temperature in air, in which case the yield was 29%. Given that the thermal reaction proceeded under an atmosphere of dinitrogen, it was assumed that dmso might act as the oxidant and [Pt(tolpy)Cl(*S*-dmso)] was formed as a minor side product. However, when dmso was excluded from the reaction mixture, both under air and under dinitrogen, **1** was also observed. This contrasts with previously reported preparations where the platinum(IV) target was obtained by from a range of platinum(II) precursors using different oxidants.[16a] Given that the reaction proceeds without added oxidant, it is reasonable to assume that oxidative addition (with concomitant production of HCl) is most likely the origin of the oxidation.
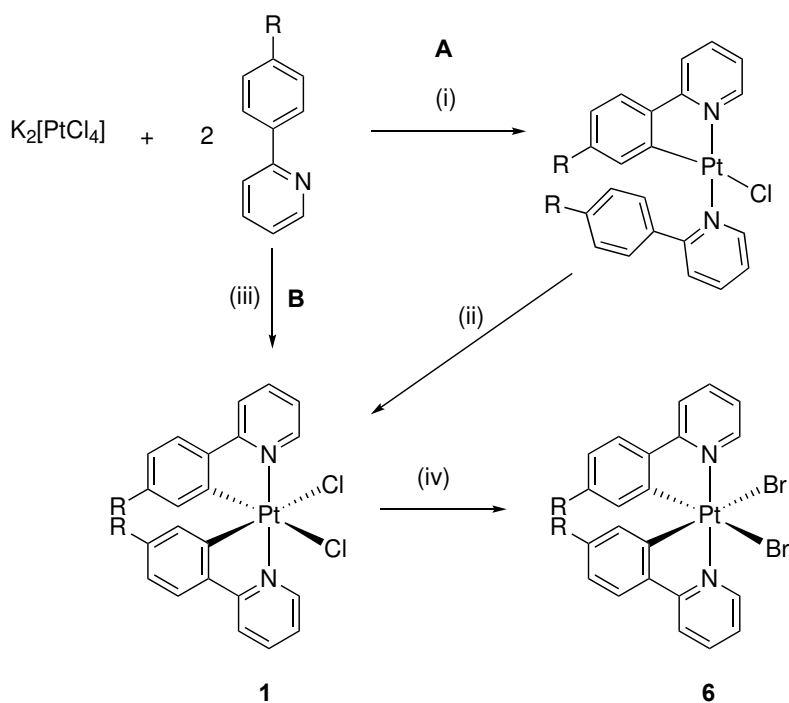
Scheme 1: Synthesis of bis-cyclometallated platinum(IV) species: Route A – literature method[8] (R = H): (i) 1:1 *tert*-butanol and water, 80 °C, 12 h; (ii) PhICl$_2$, CH$_2$Cl$_2$, r.t., 24 h ; Route B – this work (R = Me); (iii) DMSO (3 mol. equiv.), 2-ethoxyethanol, μW, 80 °C, 6 h; iv) a) AgOTf (2.5 mol. equiv.), acetone, reflux, 5 h, dark, b) excess NaBr, acetone, 50 °C, 1.5 h

An attempt was then made to prepare the analogous platinum(IV) complex of 2,5-di(4-dodecyloxyphenyl)pyridine directly from K$_2$[PtCl$_4$] (in 2-ethoxyethanol in the presence of dmso), as it was hoped that the product would be a liquid-crystalline material. However, the poor solubility of the proligand HL under conditions of reflux or microwave irradiation meant that only very low yields of the target complex were obtained. Therefore, the approach reverted to that described previously (based on route A, Scheme 1) in which the final platinum(IV) product is obtained by oxidation of a platinum(II) precursor using the iodine(III) reagent PhICl$_2$. In order to do so, the κ^2, κ^1 intermediate must be prepared directly (treatment of K$_2$[PtCl$_4$]with two molar equivalents of the substituted 2-phenylpyridine ligand under reflux in chloroform) as the alternative route (Scheme 2) requires the intermediacy of dimer **2**, which is insoluble in common laboratory solvents.[18] In this way, the desired complex **4** could be obtained in yields of 16% over two steps from K$_2$[PtCl$_4$]. Similarly, the analogous dibromoplatinum(IV) complex **5** was also prepared starting from the dichloroplatinum(IV) complex according to a literature procedure.[9a] Thus, in a one-pot reaction, treatment of **4** with silver triflate forms the *bis*(*O*-triflato)platinum(IV) complex which,

when stirred with excess sodium bromide, forms **5** (Scheme 2).[9a] The corresponding tolylpyridine complex with bromo ligands [Pt(tolpy)$_2$Br$_2$] **6** was prepared in the same manner.
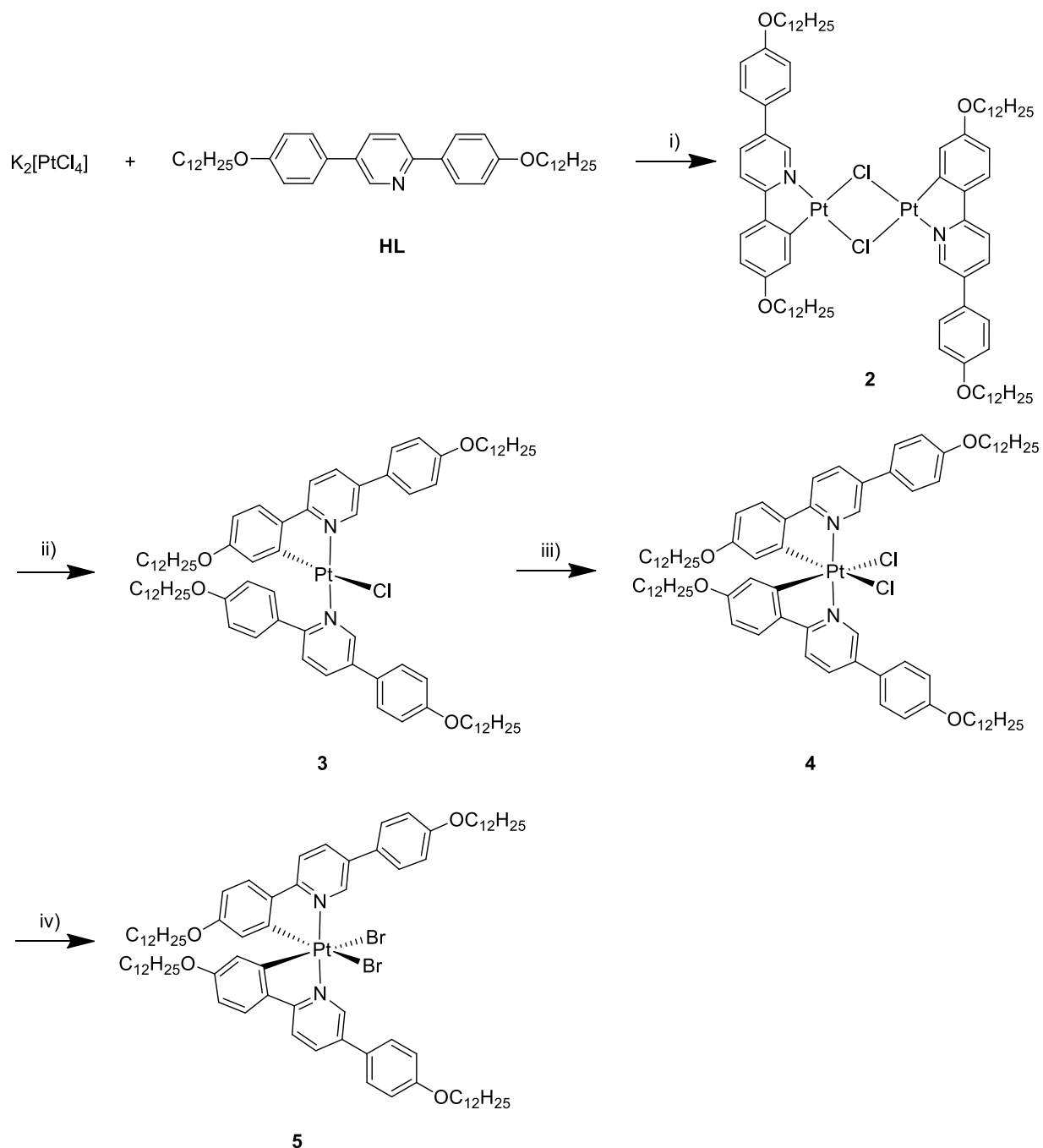
Scheme 2: Reaction scheme for the production of **2**, **3** and **4**. Reagents and conditions: i) acetic acid, reflux, 16 h; ii) 2 eq. HL, CHCl$_3$, reflux, 24 h; iii) PhICl$_2$, CH$_2$Cl$_2$, r.t., 24 h; iv) a) AgOTf (2.5 equiv.), acetone, reflux, 5 h, dark, b) excess NaBr, acetone, 50 °C, 1.5 h

Characterisation by X-Ray Single Crystal Analysis

Single crystals of **1**, its bromo analogue **6** and a homologue of the Pt^{II} complex **3** incorporating methoxy groups in place of the dodecyloxy units (**3^{Me}**) were grown, and their structures determined by single crystal X-ray diffraction (Figure 3-Figure 5). The crystal data for **1**, **3^{Me}** and **6** are summarised in Table 1. Complex **1** crystallised in the *P*–1 space group with one molecule of CHCl$_3$ per molecule of complex. The hydrogen atom of the solvent molecule forms an asymmetric, bifurcated hydrogen bond with the two ligated chloride ligands of the complex with H···Cl distances of 2.7202(6) and 2.8023(7) Å. The crystal structure shows the expected geometry, with mutually *trans N*-donor atoms and chloride ligands *trans* to the platinated carbons. The tolylpy ligands are identical, with the same Pt–N and Pt–C bond lengths (2.031(2) and 2.032(2) Å for Pt–N and 2.005(3) and 2.012(3) Å for Pt–C) and N–Pt–C bond angles (81.37(10) and 81.36(10)^{o}); the bond angles deviate from 90° due to the bite angle of the cyclometallating ligand. The Pt–Cl distances also show the chloride ligands to be equivalent (2.4365(6) and 2.4489(7) Å).

Complex **6** also crystallised in the *P*–1 space group with half a molecule of CH$_2$Cl$_2$ of crystallisation; the crystal was a non-merohedral twin and was modelled with two twin components in the refined ratio 0.543:0.457. The structure is very similar to the chloro analogue **1**, with identical tolylpy ligands in the same configuration around the platinum centre and equivalent Pt-Br bond lengths of 2.5659(8) and 2.5643(8) Å. As with **1**, the *p*-tolylpyridine ligands are identical, with the same Pt–N and Pt–C bond lengths 2.027(5) and 2.035(5) Å for Pt–N and 2.033(8) and 2.030(7) Å for Pt–C and N–Pt–C bond angles 81.6(3) and 81.31(3)^{o}. It should be noted that the Pt-C bond is significantly longer in **6** than in **1**; this bond lengthening is expected when altering the ligand *trans* to the Pt–C bond from a chloride to a bromide, with Br exerting a stronger *trans* influence than Cl.
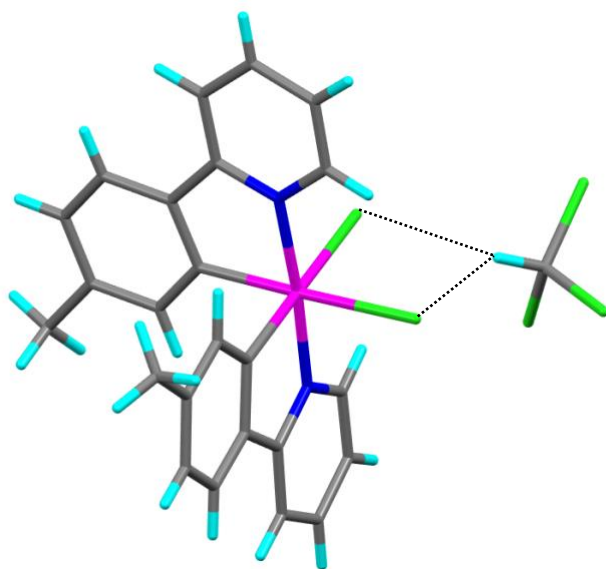
Figure 3: Molecular structure of [Pt(tolpy)₂Cl₂] **1** including a molecule of $CHCl_3$ from the solvent. The platinum atom is shown in magenta, carbon in grey, nitrogen in dark blue, chlorine in green and hydrogen in cyan.
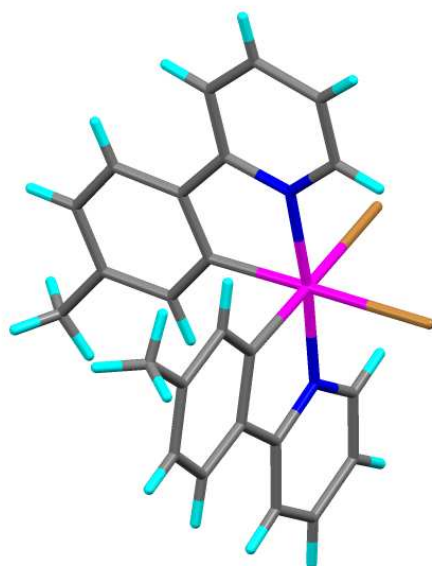
Figure 4: Molecular structure of [Pt(tolpy)₂Br₂] **6**. The molecule of disordered CH_2Cl_2 is omitted for clarity. The platinum atom is shown in magenta, carbon in grey, nitrogen in dark blue, bromine in brown, and hydrogen in cyan.

Complex **3^{Me}** crystallised with two molecules in the asymmetric unit. They differ in the conformation of the terminal methoxy group such that in one molecule, they are arranged *anti* to each other, whereas in the other they are *syn*. There is also disordered solvent in this structure and one molecule of CH_2Cl_2 was modelled in two positions and another in a large solvent void with too many positions to model accurately and so a solvent mask was used. Again, **3^{Me}** shows

the expected *trans* geometry of *N*-donors, with the lone chloride ligands *trans* to the platinated carbon. There is a slight decrease in Pt-N bond length upon cyclometallation (2.046(4) for the non-cyclometallated ligand compared to 2.014(4) Å for the cyclometallated one).
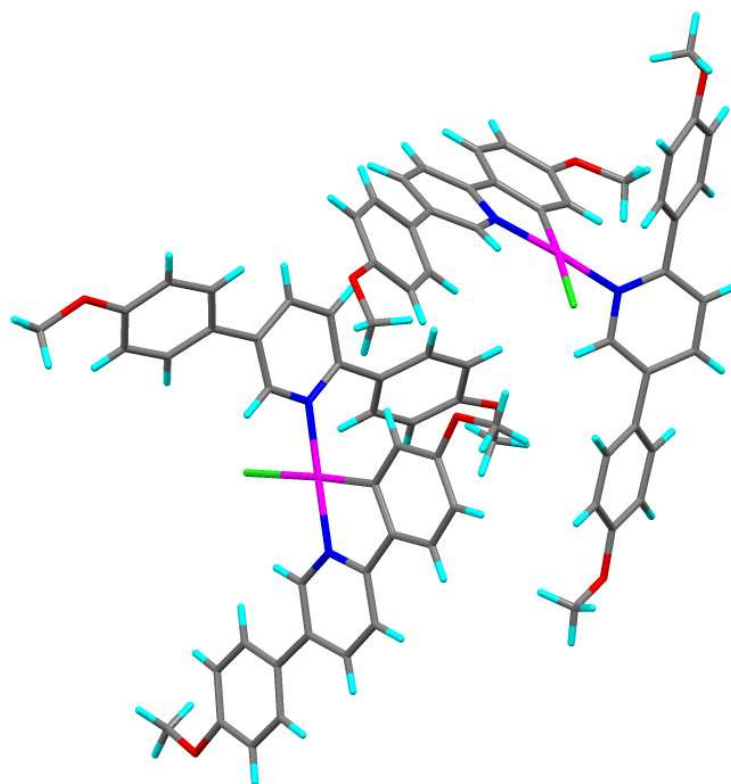
Figure 5: Molecular structure of **3^{Me}**. The molecule of disordered CH_2Cl_2 is omitted for clarity. The platinum atom is shown in magenta, carbon in grey, nitrogen in dark blue, chlorine in green, oxygen in red and hydrogen in cyan.

Table 1: Summary of X-ray diffraction data for **1**, **3^{Me}** and **6**

	1.CHCl$_3$	**3^{Me}**.CH$_2$Cl$_2$	**6**.0.5 CH$_2$Cl$_2$
Empirical formula	C$_{25}$H$_{21}$Cl$_5$N$_2$Pt	C$_{77}$H$_{68}$Cl$_4$N$_4$O$_8$Pt$_2$	C$_{24.5}$H$_{21}$Br$_2$ClN$_2$Pt
Formula weight/g mol^{-1}	721.78	1709.33	733.79
Temperature/K	110	110	110
Crystal system	triclinic	triclinic	triclinic
Space group	*P*–1	*P*–1	*P*–1
a/Å	9.8840(3)	13.4982(9)	8.2125(4)
b/Å	11.4402(4)	15.8607(7)	10.8776(8)
c/Å	12.4289(3)	17.5685(5)	13.8328(9)
α/°	93.065(3)	89.792(3)	79.447(6)
β/°	99.958(2)	82.288(4)	85.215(5)
γ/°	115.395(3)	72.526(5)	74.818(5)
Volume/Å^3	1237.53(7)	3552.6(3)	1171.60(13)

Z	2	2	2
ρ_{calc} g cm^{-3}	1.937	1.598	2.080
μ/mm^{-1}	6.227	9.112	9.528
F(000)	696.0	1692.0	694.0
Crystal size/mm^3	0.3457 × 0.1182 × 0.0329	0.389 × 0.067 × 0.037	0.32 × 0.103 × 0.08
Radiation/nm	MoKα (λ = 0.71073)	CuKα (λ = 1.54184)	MoKα (λ = 0.71073)
2θ range for data collection/°	6.726 to 60.068	6.94 to 134.16	6.598 to 60.056
Index ranges	-13 ≤ h ≤ 13, -16 ≤ k ≤ 16, -17 ≤ l ≤ 17	-16 ≤ h ≤ 16, -18 ≤ k ≤ 18, -20 ≤ l ≤ 15	-11 ≤ h ≤ 11, -15 ≤ k ≤ 15, -19 ≤ l ≤ 19
Reflections collected	13081	23781	11573
Independent reflections	7218 [R_{int} = 0.0216, R_{sigma} = 0.0376]	12643 [R_{int} = 0.0366, R_{sigma} = 0.0491]	11573 [R_{int} = n/a, R_{sigma} = 0.0449]†
Data/restraints/parameters	7218/0/300	12643/16/885	11573/0/289
Goodness-of-fit on F^2	1.061	1.019	1.062
Final R indexes [I>=2σ(I)]	R_1 = 0.0237, wR_2 = 0.0496	R_1 = 0.0370, wR_2 = 0.0943	R_1 = 0.0410, wR_2 = 0.1086
Final R indexes [all data]	R_1 = 0.0278, wR_2 = 0.0519	R_1 = 0.0462, wR_2 = 0.1024	R_1 = 0.0532, wR_2 = 0.1125
Largest diff. peak/hole / e Å^{-3}	2.19/–1.19	1.62/–1.46	2.53/–2.25
CCDC Number	1860636	1860637	1860638

† Because this structure is determined from a twinned crystal, R_{int} is not applicable.

Liquid-crystalline Properties

Complexes **4** and **5** have the potential to be liquid crystalline due to the nature of the cyclometalling ligands and by analogy with the iridium complexes in Figure 2. Both are indeed mesomorphic and their liquid-crystalline properties were characterised by polarising optical microscopy and small-angle X-ray scattering (SAXS). DSC data were not obtained as the complexes decompose on clearing and there is little useful information in the melting enthalpy alone. Thus, complex **4** shows a mesophase between 66.2 and 254.6 °C at which temperature it began to decompose; cooling back to ambient from temperatures below the clearing point does not reform the crystalline phase, rather a glassy mesophase results. Because of the decomposition at the clearing point, it did not prove possible to get good, natural textures that develop from the isotropic state, but examples of textures that were observed are given in the SI (Fig. S5). SAXS

measurements were made to establish the nature of the mesophase and showed four orders of reflection that could be indexed as a lamellar phase (Figure 6) with a *d*-spacing = 35.3 Å. There is a fifth reflection whose spacing is close to being consistent with indexation as (005), but it is of a different shape and probably with too much intensity, and so the possibility exists that it represents a short-range Pt···Pt correlation. The *d*-spacing is somewhat shorter than the length of an isolated ligand – about 45 Å – and likely the largest dimension in the complex. However, it is not clear how the complexes will pack or how space will be filled and, given the unusual shape of the molecules with respect to liquid crystal phase formation, some chain folding and/or interdigitation can be anticipated. From that point of view, it is then instructive to compare the behaviour and structural parameters with those of the dibromo analogue, **5**, which melts and clears/decomposes at very similar temperatures and also shows four orders of lamellar reflection with a fifth reflection that is again interpreted as representing a short-range Pt···Pt correlation (Figure 7). Thermal data for both complexes is shown in Table 2.
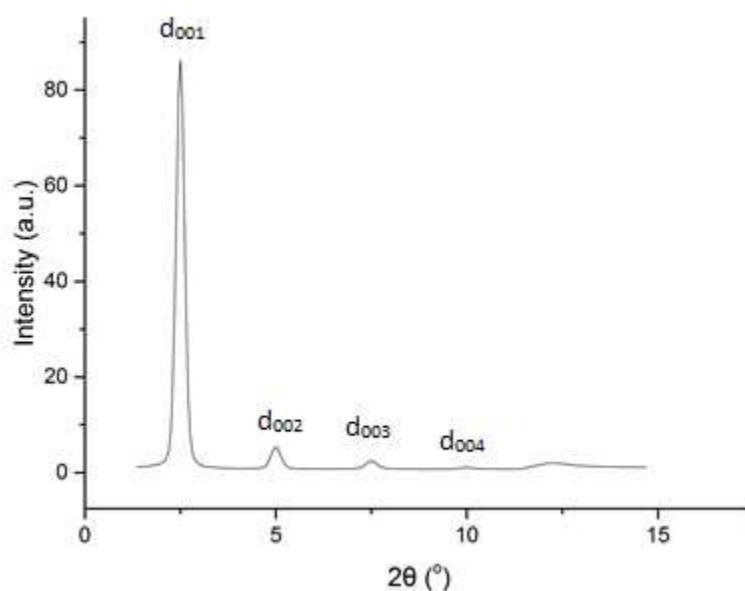

Figure 6: X-ray diffraction pattern of **4** at 189 °C showing lamellar spacing
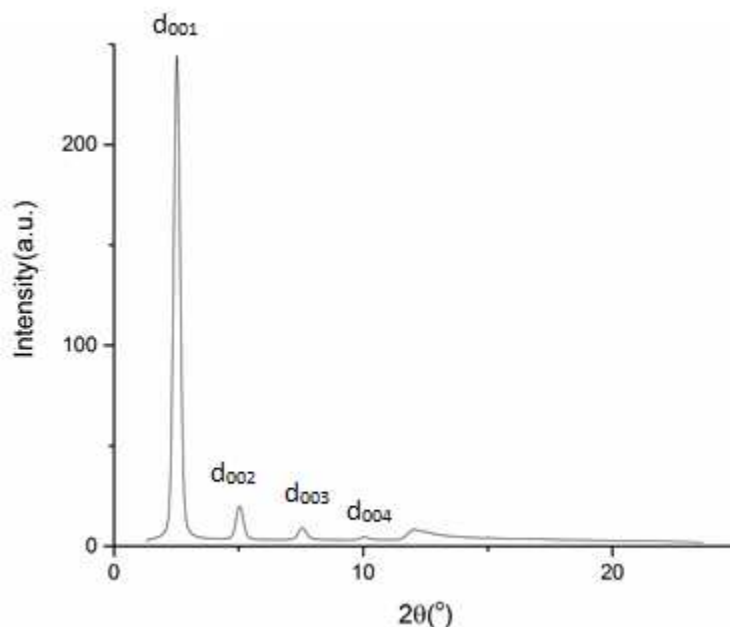
Figure 7: X-ray diffraction pattern of **5** at 178 °C showing lamellar spacing

Table 2: Thermal behaviour of complexes **4** and **5**.

Sample	Transition	T / °C
4	Cr-Lam	66.2
	Lam-Iso	254.6
5	Cr-Lam	77.6
	Lam-Iso	265.0

Owing to the anisotropic nature of the ligand concerned and for completeness, the thermal behaviour of complex **3** was investigated. Given the disposition of the κ^1-ligand to the rest of the complex, it was not anticipated that a liquid-crystalline phase would be formed and so it was with some surprise that an optical texture was observed. When viewed on the optical microscope, heating **3** shows two events at 152 and 201 °C, both of which are also observed by DSC, the former showing (first heat only) a coupled endothermic/exothermic event. Endotherms were also seen at *ca* 30 and 55 °C on the first heat, which are reversible if the sample is cycled to 100 °C, but which are not seen if the sample is heated above 152 °C. For samples heated above 201 °C, second and subsequent heating (and cooling) cycles show reversible events at 111 and 170 °C. Clearly, there is a thermally induced chemical change.

Following the first heating cycle, optical microscopy showed a texture (Figure 8a) indicative of a mesophase and the SAXS pattern (sample not purified/separated after heating to 220 °C) at 209.5 °C (Figure 8b) shows a simple lamellar arrangement with reflections corresponding to d(001), (002) and (003) all readily visible with a lamellar periodicity of 36.3 Å. These data are very similar to those recorded for **4** and **5** (Table 3) and led to the hypothesis that the κ^1-ligand had undergone some sort of oxidative addition to give complex **4** or something very similar to it.
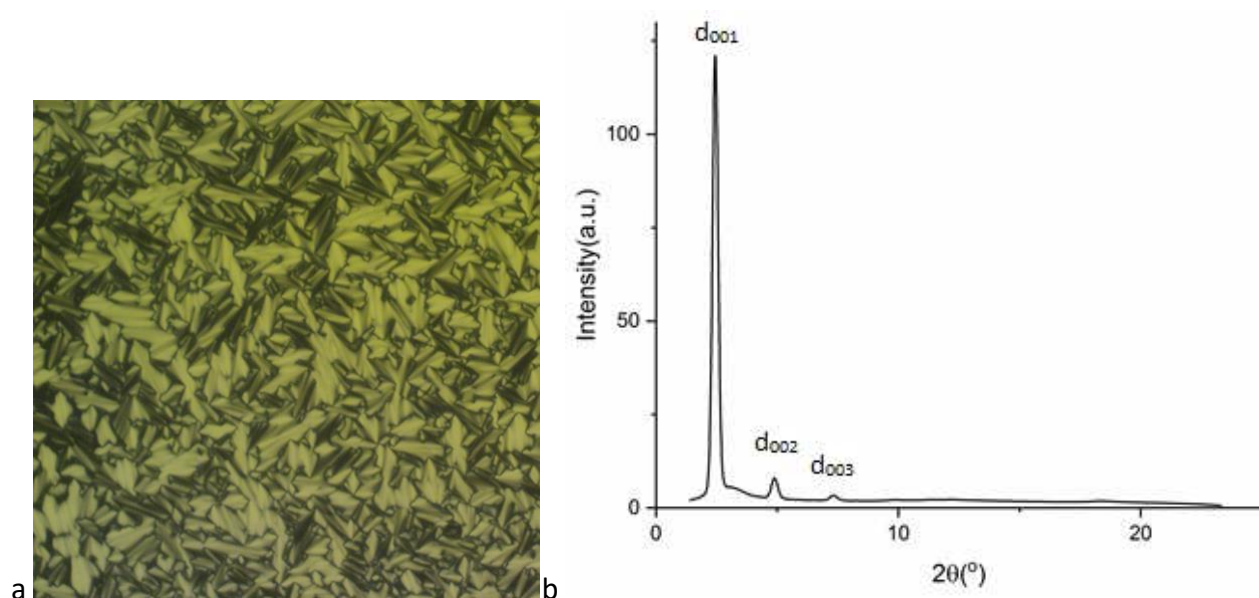
Figure 8: a) Optical micrograph of the mixture formed upon cooling **3** from the isotropic liquid (165 °C) and b) corresponding SAXS pattern 178 °C.

Table 3: X-ray diffraction data of complexes **4** and **5** (on heating) and the mixture formed upon cooling **3** from the isotropic liquid, presenting the measured and calculated spacing, and the Miller indices.

Complex	Phase	2θ (°)	d_{obs}/ Å	d_{calc}/ Å	*hkl*
4	Lam	2.50	35.3	35.3	001
	T = 189 °C	5.05	17.5	17.6	002
		7.55	11.7	11.7	003
		10.05	8.8	8.8	004
		12.03	7.3		

5	Lam	2.53	34.9	34.9	001
	$T = 178\ °C$	5.09	17.3	17.4	002
		7.62	11.6	11.6	003
		10.03	8.8	8.7	004
		12.09	7.3		
	Lam	2.43	36.3	36.3	001
		4.91	18.0	18.1	002
	$T = 178\ °C$	7.40	11.9	12.1	003
		18.35	4.8		

Examination of the ^{1}H NMR spectrum of a mixture obtained after heating **3** to 180 °C showed a complex mixture of which major components were **3**, **4** and free ligand. However, upon heating the sample further to 230 °C, the resonances for **3**, **4** and free ligand remained, but the spectra showed less of the other species in any appreciable quantity. It did not prove possible to perform a complete separation on mixtures after this thermal treatment, although a considerable quantity of free ligand could be removed by crystallisation. The ^{195}Pt NMR spectrum of the material thus purified interestingly showed resonances at, −1734, −1738 and −3169 ppm, and a less intense signal at −1303 ppm. The signal at −3169 ppm corresponds to **3**. The chemical shift of the two signals at −1734 and -1738 ppm did not vary when recording the ^{195}Pt spectra at different field strengths demonstrating that they were separate resonances and not a doublet, supporting the assignment that the latter is due to **4**. Given the large dispersion in chemical shifts seen in the ^{195}Pt NMR spectroscopy it was concluded that the species responsible for the resonance at −1734 ppm was similar to **4**. This is supported by the observation that the mixture of the two species behaves homogeneously when viewed under the optical microscope – *i.e.* they are co-miscible. *Ortho*-metallation is a subject of some interest, not least because of the relevant to C–H bond functionalisation, and in platinum(II) chemistry such reactions have been found to proceed both with retention of oxidation state and also with oxidation to platinum(IV). In relation to such

chemistry involving ppy ligands, a 2007 study by Newman *et al.* identified five possible isomers (Figure 9) arising from oxidation of [Pt(κ^2-ppy')(Cl)(κ^1-ppy'H)] (ppy'H = 2-(4-fluorophenyl)pyridine) by using ^{19}F and ^{19}F–^{195}Pt correlation NMR spectroscopy.[16b] They concluded that the ultimate isomer formed was **D**, but that **E** was formed, too, before isomerising to **D**.

A subsequent study by Whitfield and Sandford[19] using 2-phenylpyridine itself observed that the oxidation of *cis*-[Pt(ppy)$_2$] with PhICl$_2$ led to two products, the major (64%) isomer **E** (Figure 9) and a symmetric isomer (29%) that was likely one of **A** to **D** (Fig. 9). Of the symmetric possibilities, those with mutually *trans ortho*metallated carbons (Figure 9, **B** and **C**) were ruled out as unlikely owing to the strongly σ-donating nature of the carbon, while ^1H NMR data led them to propose isomer **A** as the product with quoted $\delta(^{195}Pt)$ of −1725 ppm in DMF. Later work by Juliá *et al.* examined at the same oxidation proposing **E** as the product but without mentioning possible isolation of **A**.[9a] However, oxidation of [Pt(κ^2-ppy)(Cl)(κ^1-ppyH)] (synthesis as reported by Jenkins and Bernhard[8] the ppy equivalent of complex **3** with an *ortho*metallated κ^2-C–N ppy and a neutral κ^1-*N*-ppy) using PhICl$_2$ led to isomer **D**. Thus, it is the case that both symmetric **D** and asymmetric **E** are quite readily available with small changes in reaction conditions.
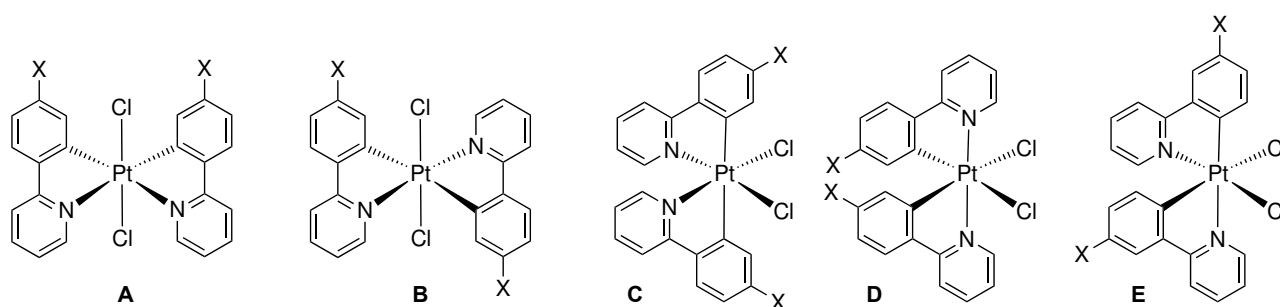
Figure 9: Different isomers of [Pt(ppy)$_2$Cl$_2$] and proposed by Newman *et al.* (X = F)[16b], Whitfield and Sandford,[19] and Juliá *et al.*[9a] (both X = H)

Given that the SAXS data obtained for thermally treated **3** correspond almost exactly to those of **4**, given also that **4** (= symmetric isomer, **D**) is identified as a product of the thermal treatment and finally that **4** and the unknown complex are co-miscible, then we propose that it is likely that

the second platinum(IV) species corresponds to the asymmetric isomer (**E**). Assignment as the *trans*-isomer is thought much less likely not least, on the grounds that isomers **A** and **D** are much less likely to be miscible.

This being the case, what is the mechanism of oxidation? The thorough study by Newman *et al.* started from [Pt(κ^2-ppy')(Cl)(κ^1-ppy'H)] and, on the basis of the conditions necessary for accessing [Pt(κ^2-ppy)$_2$], concluded that this *bis*-chelate was not an intermediate, rather that the first step was an oxidation to platinum(IV) followed by *ortho*metallation without further change in oxidation state (Figure 10). However, in this work they had accounted for the stoichiometry of the platinum(IV) product and so had added chloride (as KCl) as well as an oxidant (hydrogen peroxide) to this solution-phase reaction. In the present case, the oxidation is occurring in the solid state/melt without added oxidant or chloride, and proceeds under atmospheres of both air and argon.
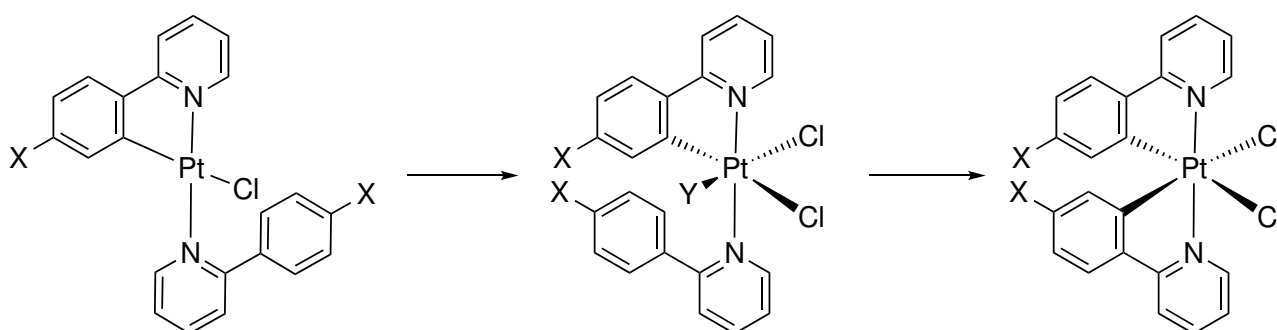
Figure 10: Mechanistic pathway proposed by Newman *et al.* for the oxidation of [Pt(κ^2-ppy)(Cl)(κ^1-ppyH)] to *cis*-[Pt(κ^2-ppy')$_2$Cl$_2$].[16b]

However, as noted above, this requires two molar equivalents of **3** to generate one molar equivalent of **4** (and its proposed isomer) in order to satisfy the stoichiometry. As such, formation of **4** must be somehow bimolecular and so it is not unsurprising that both free ligand and other species are seen by NMR spectroscopy post thermal treatment. It is tempting to suppose that under these solvent-free, thermal conditions under argon, oxidation occurs though either an intra- or intermolecular cyclometallation or disproportionation. The fact that no platinum black was observed would appear to disfavour the latter process. Therefore, an initial *ortho*-metallation

with oxidation of **3** could occur to form a five-coordinate complex which scavenges a chloride from another molecule of **3** forming **4** and leading to the decomposition of the second, now coordinatively unsaturated complex. The rotation available about the Pt–N single bond could account for the formation of the two isomers, or it could be that the less symmetric isomer (Figure 9, **E**) forms in preference and is gradually isomerised to **D** as proposed by Newman *et al.*[16b] Elucidation of this mechanism is, however, outwith the scope of this paper.

Absorption spectra

The UV-visible absorption spectra of the platinum(IV) compounds **1**, **4**, and **5**, and of the precursor platinum(II) complex **3**, were recorded in CH_2Cl_2 at room temperature (Figure 11-Figure 13 and Table 4). The lowest-energy absorption band of the yellow platinum(II) complex **3** is centred at 408 nm (ε = 10400 M^{-1} cm^{-1}), with a series of more intense bands in the UV region. The low-energy band is quite typical of cyclometallated platinum(II) complexes,[5c, 20] and is attributed to $d_{Pt}/\pi_{N^\wedge C} \rightarrow \pi^*_{py}$ charge-transfer transitions. In contrast, the lowest-energy absorption maxima of the platinum(IV) complexes are all at shorter wavelengths, in the UV region. This substantial blue-shift is consistent with the lowering in energy of the metal-based d orbitals upon increasing oxidation state: a change to a more purely ligand-based $\pi \rightarrow \pi^*$ excited state is anticipated. It is notable, however, that the bands displayed by the platinum(IV) complexes **4** and **5** – featuring the dodecyloxy and dodecyloxyphenyl substituents – are red-shifted relative to the parent complex **1**: the absorption energy is decreased by around 3200 cm^{-1}. Such a trend can be rationalised in terms of the destabilisation of the π orbitals of the *N^C*-coordinating ligands upon extension of the conjugation and incorporation of electron-donating substituents.

Figure 11: *(a)* Absorption (black line), excitation (dashed purple) and emission (red) spectra of complex **3** in CH₂Cl₂ at 298 K and the emission spectrum in EPA at 77 K (blue). *(b)* The emission spectrum of powdered **3** at 298 K.

Figure 12: Absorption (black line) and emission (red) spectra of complex **1** in CH₂Cl₂ at 298 K and its emission spectrum in EPA at 77 K (blue).
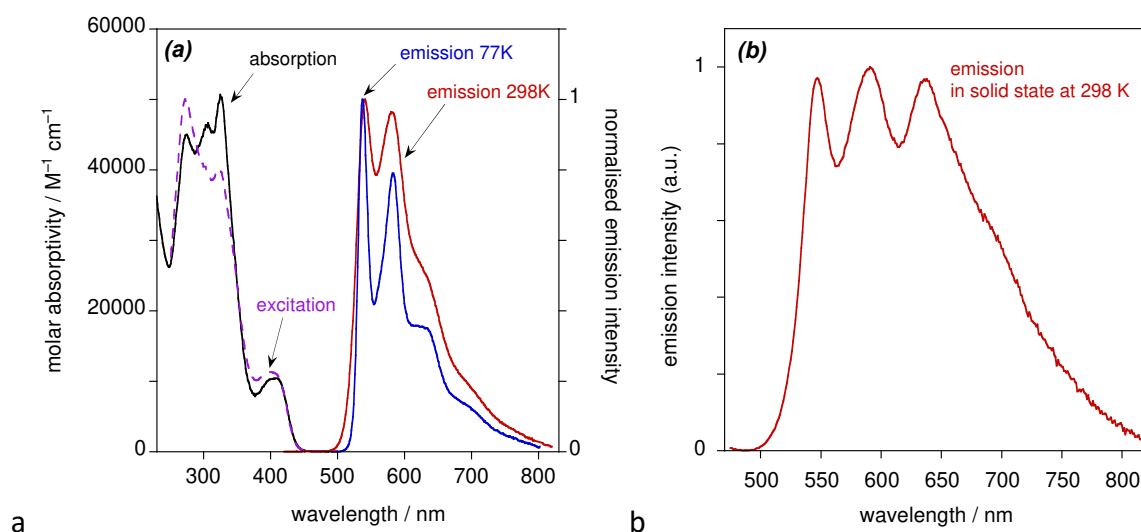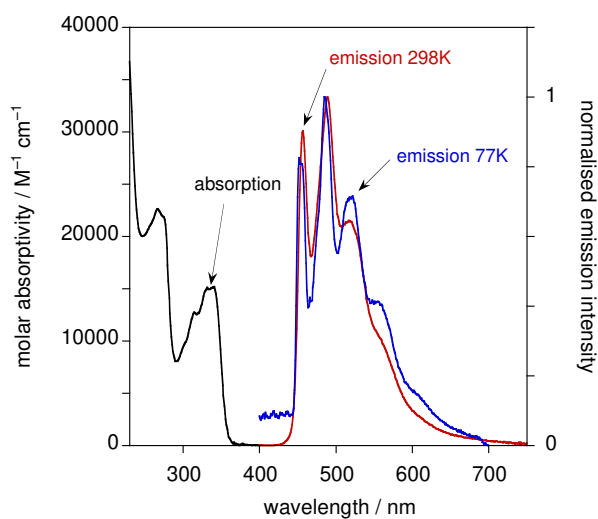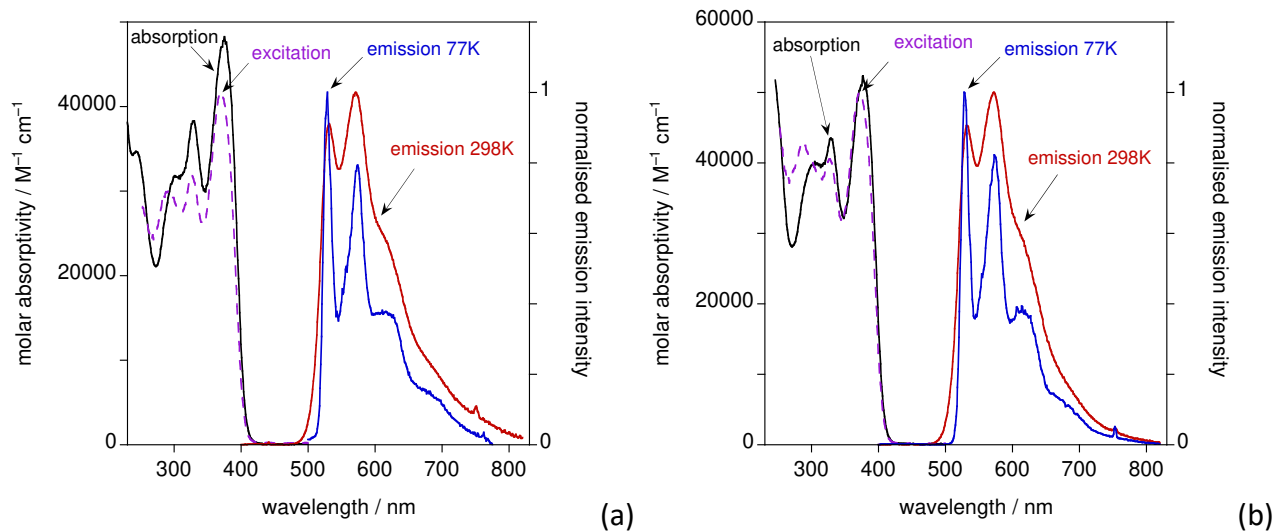
Figure 13: Absorption (black line), excitation (dashed purple) and emission (red) spectra of: (a) of complex **4** in CH$_2$Cl$_2$ at 298 K and its emission spectrum in EPA at 77 K (blue) and (b) complex **5** in CH$_2$Cl$_2$ at 298 K and its emission spectrum in EPA at 77 K (blue).

Table 4: Photophysical data for complexes **1, 3, 4, 5** and **6** [a]

Complex	Absorption λ_{max} / nm (ε / M^{-1} cm^{-1})	Emission λ_{max} / nm	$10^2\,\Phi_{lum}$ [b]	τ / ns degassed	$10^3\,k_r$ / s^{-1} [c]	$10^3\,\Sigma k_{nr}$ / s^{-1} [c]	$10^7\,k_Q$ (O$_2$) M^{-1}s^{-1} [d]	Emission 77 K [e] λ_{max} / nm	τ / ns
1	266 (29700), 274 (28800), 315 (13200), 335 (14900)	457, 489, 518, 562	7.0	72,000 [5,000](f)	0.97	13	8.5	452, 486, 519, 555, 613	318,000
3	274 (48900), 306 (49600), 326 (52700), 408 (10400)	541, 581, 631sh, 706sh	22[g]	28,000 [510]	7.9	28	88	537, 583, 626, 697	38,000
4	244 (41000), 302 (42000), 329 (43200), 375 (48200)	532, 571, 621sh	9.0	230,000 [1,100]	0.39	4.0	41	528, 574, 616, 684	336,000
5	306 (54400), 329 (49000), 376 (52400)	532, 572, 618sh	11	230,000 [1,500]	0.48	3.9	30	528, 574, 615, 678	360,000
6	268 (26500), 315 (12700), 333 (12900), 344 (13500)	457, 490, 518, 562	0.6	--[h]	--	--	--[i]	452, 470, 477, 486, 515, 525, 554	

(a) In degassed CH$_2$Cl$_2$ at 295 ± 3 K, except where indicated otherwise. (b) Quantum yields measured relative to aqueous [Ru(bipy)$_3$]Cl$_2$. (c) Radiative k_r and non-radiative Σk_{nr} rate constants estimated from quantum yield and lifetime: $k_r = \Phi / \tau$, $k_r = (1-\Phi) / \tau$. (d) Bimolecular Stern-Volmer constant for quenching by molecular oxygen. (e) In diethyl ether − isopentane − ethanol (2:2:1 v/v). (f) This aerated value of 5 μs is subject to considerable uncertainty (and consequently also the k_Q(O$_2$) value), as it is recorded using a microsecond flashlamp source to access the necessary short wavelength of excitation. (g) PLQY in solid state was also measured for this sample, ☐ = 0.02. For the platinum(IV) complexes, only very weak emission was observable in the solid state. (h) The lifetime of this complex could not be recorded due to the very low absorption at wavelengths available for TCSPC measurements. (i) The intensity of emission decreases by a factor of approximately 2.5 for an air-equilibrated as compared to a deoxygenated solution.

Luminescence

Based on the emerging literature of platinum(IV) compounds with cyclometallating ligands described in the introductory section, complexes **1, 4** and **5** were expected to be luminescent. The excitation and emission spectra of these complexes were measured in deaerated CH_2Cl_2 at 298 K and in frozen diethyl ether – isopentane – ethanol (2:2:1 v/v; referred to as EPA) at 77 K (Figure 12 and Figure 13). The data collected are summarised in Table 4, together with corresponding properties of the platinum(II) complex **3** (Figure 11a).

The platinum(II) complex, **3**, is strongly luminescent in deoxygenated dichloromethane solution, in the green-yellow region of the spectrum. The vibrationally structured emission spectrum has a λ_{max} for the (0,0) band of 541 nm (Figure 8a); the quantum yield of luminescence Φ is 0.22 and the lifetime τ is 28 µs. The efficient room-temperature phosphorescence of [Pt(N^C)(L^X)] and [Pt(N^C) (X)(L)] complexes has become well-established over the past 20 years.[5c, 20] The quantum yield and lifetime of **3** are, however, significantly higher and longer, respectively, than many such complexes. A suitable simpler model complex with which to compare **3** is [Pt(ppy)Cl(Hppy)], first reported by Ford and co-workers in 1995.[21] That complex displays blue-shifted emission, λ_{max}(0,0) = 489 nm, with a much shorter lifetime (641 ns). The difference in emission energy between **3** and this model complex mirrors the trend to lower-energy absorption upon introduction of the dodecyloxyphenyl substituents discussed above. A similar trend to brighter and longer-lived luminescence on increasing the extent of ligand congugation has been seen in [Pt(N^C)(acac)] complexes (*e.g.*, ongoing from N^C = ppy to thienylpyridine) and probably reflects an increase in the energy gap between the emissive state and higher-lying deactivating states (*e.g.* metal-based d-d states) as the emissive excited state energy decreases.[22]

Complex **3** is also luminescent in the solid state (powdered form), showing a broad spectrum across the orange-red region, albeit featuring some vibrational structure (Figure 11b). It is likely that face-to-face intermolecular interactions lead to aggregate species under these conditions,

which contribute additional broad emission bands in the red region, superimposed on the monomer emission bands.[23] The quantum yield in the solid state is 0.02.

The luminescence of the platinum(IV) complex [Pt(tolpy)$_2$Cl$_2$] **1** has been briefly described previously,[16a] although the quantum yield was not reported. We have determined a quantum yield of 0.07 in deoxygenated dichloromethane solution. The spectrum displays a high degree of vibrational structure with λ_{max}(0,0) at 457 nm (Figure 12); the (0,1) band is the vibrational component of highest intensity. The corresponding bromo complex [Pt(tolpy)$_2$Br$_2$] **6** has essentially identical spectral and temporal excited state properties as the chloro analogue at 77 K, and an essentially identical spectral profile at room temperature, but its quantum yields at room temperature is an order of magnitude lower. This broadly mirrors the difference between [Pt(ppy)$_2$Cl$_2$] and [Pt(ppy)$_2$Br$_2$], described by Julià *et al.*[9b] A 60-fold increase in k_{nr} in the bromo complex was attributed to higher-lying p$_{hal} \rightarrow \pi^*_{ppy}$ and/or p$_{hal} \rightarrow$ dσ^*_{Pt} states becoming thermally accessible when hal = Br, and serving as a pathway of non-radiative decay.

The platinum(IV) complexes **4** and **5** are also quite strongly luminescent. The emission is red-shifted relative to that of **1**. Based on the positions of the (0,0) bands (Table 4), it can be seen that the energy of the emissive triplet state is lowered by around 3100 cm^{-1} compared to **1**, a very similar value to the corresponding stabilisation of the lowest-energy spin-allowed band seen in absorption. Though the quantum yields are only marginally higher than for **1** (Φ = 0.09 and 0.11 for **4** and **5**, respectively), their emission lifetimes of 230 μs are around three times longer, indicative of a lower radiative rate constant, k_r.

These observations are consistent with other recent studies on platinum(IV) luminescence in related complexes, which assign the emission to largely ligand-localised triplet states, with relatively little participation of the metal orbitals.[6, 9a, 24] Appending the alkyloxyphenyl substituents will evidently extend the ligand conjugation further, increasing the mismatch between ligand π and metal d orbitals, resulting in less metal character to the excited state, less efficient spin-orbit coupling, lower radiative rate constants, and longer lifetimes. Interestingly,

however, non-radiative decay processes must be attenuated in **4** and **5** compared to **1**, otherwise the quantum yield would be compromised by the lower k_r values.

The minimisation of non-radiative decay pathways is typically favoured by high structural rigidity and minimal distortion between the S_0 and T_1 states. The lack of substantial distortion in the current complexes is supported by the observation that, in a rigid glass at 77 K, the emission maxima are blue-shifted by as little as 4 nm (Figure 11-Figure 13).

The similarity in the luminescence properties of the chloro and bromo complexes **4** and **5** is striking (Figure 13 and Table 4). The emission maxima and lifetimes are the same, and the luminescence quantum yields are within the uncertainty on the measurement. Apparently, the identity of the halide has essentially no influence on the emissive excited state. This observation of similar quantum yields and lifetimes for these two complexes contrasts strikingly with on the difference between **1** and **6**, and the previously reported difference between [Pt(ppy)$_2$Cl$_2$] and [Pt(ppy)$_2$Br$_2$], both of which revealed a large drop in the quantum yield and lifetime for the bromo relative to chloro.[9a] As noted above, this was attributed to the influence of higher-lying, deactivating p$_{hal} \rightarrow \pi^*_{ppy}$ and/or p$_{hal} \rightarrow d\sigma^*_{Pt}$ states becoming thermally accessible when hal = Br. In the present instance of complex **5**, on the other hand, the excited state energy is much lower than that of [Pt(ppy)$_2$Br$_2$] {E_T = 18800 and 22200 cm^{-1} respectively, based on the (0,0) bands} and so such potentially deactivating states may remain thermally inaccessible.

In the solid state, the platinum(IV) complexes **4** and **5** show only very weak emission. Clearly, their low radiative rate constants, and hence long excited state lifetimes, will favour efficient intermolecular self-quenching processes. Such quenching effects occur even for well-known iridium(III) phosphors when in the neat solid state (as opposed to the doped materials used in devices), despite having much higher radiative decay rates than these platinum(IV) complexes. The elimination of such intermolecular processes remains a challenge in the use of non-doped phosphorescent molecular materials.

Computational Chemistry

Time-dependent density functional theory (TD-DFT) was employed to rationalise the absorption

spectra of complexes **1** and **4**. Full details of the methodology employed are presented in the E.S.I.

In order to aid computation efficiency, the $OC_{12}H_{25}$ chains in **4** were replaced by OCH_3 groups in

the model compound **4^{Me}**. As shown in Table 5, the calculations reproduce some of the pertinent

experimental features and there is a reasonable match between the experimental and predicted

energies of the transitions. For example, the lowest energy feature in the spectrum is red-shifted

on changing from **1** to **4**, a trend that is reproduced computationally by comparing **1** and **4^{Me}**.

For **1**, the lowest-energy band involves a number of related transitions involving a combination of

the filled HOMO (115) and HOMO-1 (114) and vacant the LUMO (116) and LUMO+1 (117) orbitals.

The two filled orbitals are composed of two chloride non-bonded pairs and a contribution from

the π-system of the 2-phenylpyridine ligand, whereas the LUMO and LUMO+1 are best viewed as

ligand-based π*-orbitals (Figure 14). The next series of transitions also involved transfer to LUMO

and LUMO+1, the parent orbitals in these cases having a similar composition to the HOMO and

HOMO-1 (orbitals 113 and 112), whereas orbitals 111 and 110 have a contribution from a metal *d*-

orbtial and the two halide non-bonded pairs.

In the case of **4^{Me}** the situation is similar, but the two occupied orbitals involved in the lowest-

energy transition (HOMO, 179 and HOMO -1, 178) are solely 2-phenylpyridine-based π-orbitals.

Again, the acceptor orbitals (LUMO, 180 and LUMO+1, 181) are corresponding ligand-based π*-

orbitals. The filled orbitals for the next series of transitions (177, 176 and 175) are mostly

composed from chloride non-bonded pairs with little contribution from the 2-phenylpyridine

system.

Therefore, from a more qualitative perspective, the addition of the second phenyl substituent to

form the 2,5-di(4-alkoxyphenyl)pyrdine ligand increases the energy of the π-based HOMO orbital

so that there is little mixing with the chloride non-bonded pairs. Indeed, the transitions in both **1** and **4^{Me}** are essentially identical (see ESI). These theoretical outcomes corroborate our interpretation of the emission data discussed above, in terms of the increased conjugation lowering the metal character in the excited state.

In the bromo-containing compound **5**, which was modelled as **5^{Me}**, the calculations indicate that the energy of transitions are similar to **4**, as observed experimentally, although now the occupied orbitals involved in the lowest-energy transition (197, 195 and 194) have bromide non-bonded pair character. The acceptor orbitals, LUMO (198) and LUMO+1 (199) are still ligand π^*-based.

Table 5: Summary of experimental and DFT-predicted transitions for complexes **1**, **4** and **4**[Me], and **5** and **5**[Me]. Only transitions with an oscillator strength >0.01 and orbital contributions >10% are listed. See ESI for additional transitions.

Complex	Experimental Energy / nm	Calculated Energy / nm	Oscillator strength	Occupied orbital(s)	Virtual orbital(s)	Coefficient / %
1	335	342	0.0233	114	117	53.6
				115	116	34.0
		341	0.0552	115	117	66.2
				114	116	19.8
4/4[Me†]	375	368	0.766	179	180	63.0
				178	181	26.8
		367	0.396	179	181	48.9
				178	180	41.0
		357	0.0236	178	181	57.0
				179	180	27.2
5/5[Me†]	376	380	0.0455	197	199	61.1
				195	199	30.5
		377	0.131	197	199	62.0
				195	199	26.2
		370	0.459	196	198	67.9
				194	198	12.6
		368	0.244	196	199	65.7
				195	198	12.0
		355	0.0484	195	198	52.3
				197	198	22.8
				196	199	13.7
		354	0.0435	195	199	41.9
				197	199	28.3
				196	198	18.2
		352	0.0136	194	199	70.2
				196	199	11.7
		351	0.151	194	198	69.4
				195	199	17.9
		348	0.225	193	198	78.7
				192	199	10.6

[†]Data for **4** and **5** are experimental, while those for **4**[Me] and **5**[Me] arise from calculation.

-2.027 —— 117
-2.053 —— 116
LUMO

-1.824 —— 181
-1.855 —— 180
LUMO

-1.855 —— 199
-1.891 —— 198
LUMO

HOMO

-5.855 ⫩⫩ 179
-5.864 ⫩⫩ 178

HOMO

-5.857 ⫩⫩ 197
-5.879 ⫩⫩ 196

-6.019 ⫩⫩ 195
-6.163 ⫩⫩ 194

HOMO
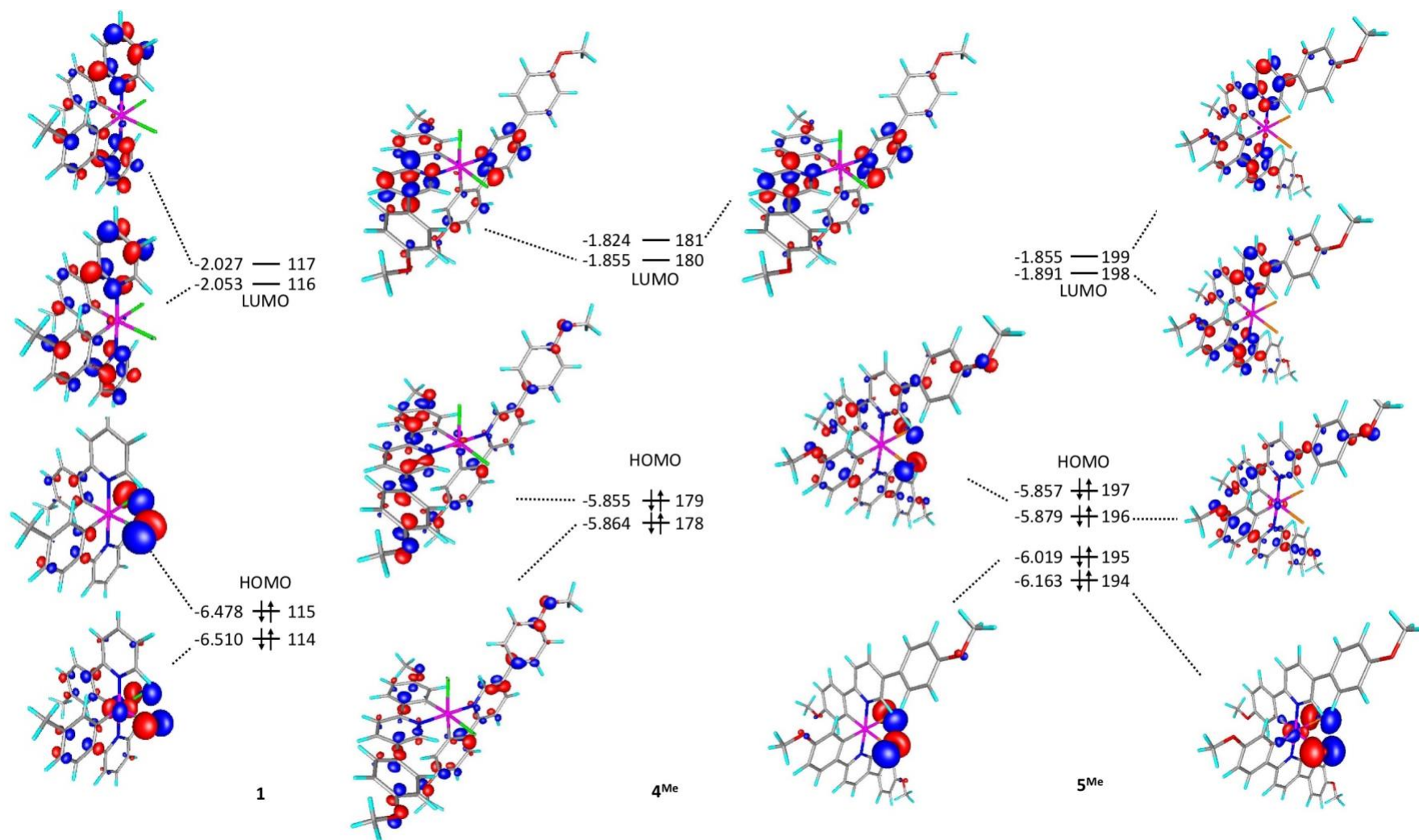-6.478 ⫩⫩ 115
-6.510 ⫩⫩ 114

1

4^Me

5^Me

Figure 14: Frontier orbitals for complexes **1**, **4^Me** and **5^Me**.

Conclusion

In summary, we have developed a novel, one-pot synthesis to the established species [Pt(tolpy)$_2$Cl$_2$]. We believe this synthetic procedure could be successfully applied to other complexes with simply functionalised phenylpyridine ligands, although it proves to be less applicable with more functionalised 2,5-diphenylpyridine ligands. The introduction of directional anisotropy into platinum(IV) system through the utilisation of 2,5-di(4-dodecyloxyphenyl)pyridine ligands results in species which are liquid crystalline and triplet emitters in the blue region. The same is true of the bromide analogue and the nature of the emissive state appears to be similar for both halides. To the best of our knowledge, **4** and **5** are the first reported platinum(IV) complexes of this nature to show liquid crystallinity, and offer the potential for a new class of emissive materials.

Experimental

General Considerations, Materials and Instrumentation

Unless stated otherwise, reactions were carried out at room temperature under ambient conditions. All reagents were procured through common commercial sources and used without further purification. PhICl$_2$,[8] 2,5-di(4-dodecyloxyphenyl)-pyridine and compound **2**[18] were prepared according to established literature procedures.

^{1}H NMR spectra were measured on a Jeol ECS400 spectrometer operating at 400 MHz with chemical shifts referred to residual non-deuterated CHCl$_3$ signals. [195]Pt NMR spectra were measured on Bruker 500 AVANCE II spectrometer operating at 107 MHz. CHN elemental analysis was carried out using an Exeter Analytical Inc. CE-440 Analyser and Sartorius S2 analytical balance; calibration was performed against acetanilide standards and checked by the use of *S*-benzyl thiouronium chloride as internal standard. A CEM Discover S-class microwave was used in the synthesis of **1.**

Polarising optical microscopy was carried out using an Olympus BX50 polarizing microscope equipped with a Linkam scientific LTS350 heating stage, Linkam LNP2 cooling pump, and Linkam TMS92 controller, differential scanning calorimetry was performed on a Mettler DSC822^e using Mettler STAR-E software, which was calibrated before use against indium and zinc standards under an atmosphere of dry nitrogen. Small angle X-ray scattering was recorded using a Bruker D8 Discover equipped with a temperature controlled, bored graphite rod furnace, custom built at the University of York. Cu-K$_\alpha$ (λ = 0.154056 nm) radiation was used, generated from a 1 μS microfocus source. Diffraction patterns were recorded on a 2048 $\times$ 2048 pixel Bruker VANTEC 500 area detector set at a distance of 121 mm from the sample, allowing simultaneous collection of small angle and wide angle scattering data. Samples were measured in 1 mm capillary tubes in a magnetic field of *ca* 1 T.

The absorption spectra of the complexes were measured in solution in CH_2Cl_2 in 1 cm pathlength quartz cuvettes using a Biotek Instruments XS spectrometer. Emission spectra were recorded using a Jobin Yvon Fluoromax-2 spectrometer equipped with a Hamamatsu R928 photomultiplier tube (PMT). For the measurements at 298 K, the solutions were contained within 1 cm pathlength quartz cuvettes modified for connection to a vacuum line. Degassing was achieved via a minimum of three freeze-pump-thaw cycles whilst connected to the vacuum manifold; final vapour pressure at 77 K was < 5 x 10^{-2} mbar, as monitored using a Pirani gauge. Luminescence quantum yields were determined using aqueous [Ru(bipy)$_3$]Cl$_2$ as the standard (Φ = 0.028 in air-equilibrated aqueous solution).[25] Emission spectra at 77 K were recorded in a glass of EPA (= diethyl ether / isopentane / ethanol, 2:2:1 v/v) in 4 mm diameter tubes held within a liquid-nitrogen-cooled quartz dewar. The emission spectrum of complex **3** in the solid state was recorded by means of an integrating sphere attached to a Jobin Yvon Fluorolog instrument through optical fibres. The powdered sample was contained within a Spectralon holder of 1 cm diameter. The quantum yield was evaluated using a sample of finely powdered BaSO$_4$ as a non-emissive blank. Scattered light at the excitation wavelength for sample and blank was measured using a neutral density filter of O.D. = 2, whilst the emission region was monitored in the absence of the filter. The luminescence

lifetimes of the complexes in deoxygenated solution and at 77 K were measured by multi-channel scaling following excitation into the lowest-energy absorption band using a microsecond pulsed xenon lamp. The emitted light was detected at 90˚ using a Peltier-cooled R928 PMT after passage through a monochromator. The lifetimes in air-equilibrated solution (< 10 μs) were measured by time-correlated single photon counting (TCSPC), following excitation at 374 nm with a pulsed laser diode. We were unable to determine the lifetime of **6** due to its negligible absorption at this wavelength.

Diffraction data were collected at 110 K on an Oxford Diffraction SuperNova dual-source X-ray diffractometer with Mo-K$_\alpha$ radiation (λ = 0.71073 Å) (**1** and **6**) or CuKα (λ = 1.54184) (**3^{Me}**) using a EOS CCD camera. The crystal was cooled with an Oxford Instruments Cryojet. Diffractometer control, data collection, initial unit cell determination, frame integration and unit-cell refinement was carried out with 'Crysalis'.[26] Face-indexed absorption corrections were applied using spherical harmonics, implemented in SCALE3 ABSPACK scaling algorithm.[27] OLEX2[28] was used for overall structure solution, refinement and preparation of computer graphics and publication data. Within OLEX2, the algorithms used for structure solution were Superflip charge-flipping[29] (**1**) and ShelXT[30] (**3^{Me}** and **6**). Refinement by full-matrix least-squares used the SHELXL-97[31] algorithm within OLEX2.[28] All non-hydrogen atoms were refined anisotropically. Hydrogen atoms were placed using a 'riding model' and included in the refinement at calculated positions.

All calculations were performed using the TURBOMOLE V6.4 package using the resolution of identity (RI) approximation.[32] Initial optimisations were performed at the (RI-)BP86/SV(P) level, followed by frequency calculations at the same level. All minima were confirmed as such by the absence of imaginary frequencies. Single-point and TD-DFT calculations on the (RI-)BP86/SV(P) optimised geometries were performed using the hybrid PBE0 functional and the flexible def2-TZVPP basis set with a 60-electron effective core potential. Energies, xyz coordinates and the first 50 lines of the vibrational spectra are presented in Supplementary Information.

Synthetic procedures and characterisation data

[Pt(tolpy)$_2$Cl$_2$] **(1)**: K$_2$[PtCl$_4$] (0.073 mmol, 30.5 mg) dissolved in the minimum volume of hot water was added to a mixture of 2-*p*-tolylpyridine (0.42 mmol, 0.024 mL) and DMSO (0.21 mmol, 0.015 mL) in 2-ethoxyethanol (10 mL). The reaction mixture was heated with stirring at 80 °C for 6 hours under microwave conditions. The resulting precipitate was isolated by filtration and washed with water and cold methanol to afford the pure product. Yield= 13 mg (29 %). ^{1}H NMR (400 MHz, CDCl$_3$): δ = 10.00 (2H, d, $^3J_{HH}$ = 6.0 Hz, $^3J_{HPt}$ = 29.0 Hz), 8.06 (2H, td, $^3J_{HH}$ = 7.6 Hz, $^4J_{HH}$ = 1.2 Hz), 7.92 (2H, d, $^3J_{HH}$ = 8.0 Hz), 7.48 (2H, d, $^3J_{HH}$ = 8.0 Hz), 7.45 (2H, td, $^3J_{HH}$ = 6.4 Hz, $^4J_{HH}$ = 1.2 Hz), 6.92 (2H, d, $^3J_{HH}$ = 8.0 Hz), 5.83 (2H, s, $^3J_{HPt}$ = 33 Hz), 2.10 (6H, Me, s); CHN elemental analysis: observed (calculated): %C 47.61 (47.85), %H 3.29 (3.35), %N 4.55 (4.65).

[Pt(κ^2-N^C-L)Cl(κ^1-N^C-LH)] **(3)**: CHCl$_3$ (70 mL) was added to compound **2** (0.293 mmol, 450 mg) and 2,5-di(4-dodecyloxyphenyl)-pyridine (0.584 mmol, 333.9 mg). The resulting reaction mixture heated at reflux for 24 hours. The solution was cooled to room temperature, filtered through Celite® to remove any residual compound **2** and the solvent removed under reduced pressure. The residue was washed with ice-cold CHCl$_3$, the filtrate collected and the solvent removed under reduced pressure. The residue was recrystallized from CHCl$_3$/propanone to yield the pure product. Yield = 285 mg (68 %). ^{1}H NMR (400 MHz, CDCl$_3$): δ = 9.84 (1H, d, $^4J_{HH}$ = 2.0 Hz), 9.45 (1H, d, $^4J_{HH}$ = 2.0 Hz), 8.14 (2H, d, $^3J_{HH}$ = 8.8 Hz), 8.03 (1H, dd, $^3J_{HH}$ = 8.4 Hz, $^4J_{HH}$ = 2.0 Hz), 7.86 (1H, dd, $^3J_{HH}$ = 8.4 Hz, $^4J_{HH}$ = 2.0 Hz), 7.63 (1H, d, $^3J_{HH}$ = 8.4 Hz), 7.56 (4H, dd, $^3J_{HH}$ = 8.8 Hz, $^4J_{HH}$ = 1.6 Hz), 7.42 (1H, d, $^3J_{HH}$ = 8.4 Hz), 7.28 (1H, d, $^3J_{HH}$ = 8.4 Hz), 6.97 (2H, d, $^3J_{HH}$ = 8.8 Hz), 6.96 (2H, d, $^3J_{HH}$ = 8.4 Hz), 6.86 (2H, d, $^3J_{HH}$ = 8.8 Hz), 6.55 (1H, dd, $^3J_{HH}$ = 8.4 Hz, $^4J_{HH}$ = 2.4 Hz), 5.77 (1H, d, $^4J_{HH}$ = 2.4 Hz), 3.98 (4H, t, $^3J_{HH}$ = 6.8 Hz), 3.89 (2H, t, $^3J_{HH}$ = 6.8 Hz), 3.75 (2H, m), 1.79 (4H, m), 1.71 (2H, m), 1.65 (2H, m), 1.46 (4H, m), 1.25 (64 H, broad m), 0.87 (12H, m); ^{195}Pt NMR (107 MHz, CDCl$_3$): δ = -3167 ppm; CHN elemental analysis: observed (calculated): %C 68.55 (68.90), %H 8.44 (8.53), %N 1.89 (1.96)

[Pt(κ^2-N^C-L)$_2$Cl$_2$] **(4)**: Compound **3** (0.68 mmol, 100 mg) and PhICl$_2$ (1.36 mmol, 37.5 mg) were dissolved in CH$_2$Cl$_2$ (60 mL) and stirred for 24 hours. The solvent was subsequently removed under

reduced pressure and the residue recrystallized from toluene/methanol to yield the pure product. Yield = 71.8 mg (70 %). ^{1}H NMR (400 MHz, CDCl$_3$): δ = 10.18 (2H, d, $^4J_{HH}$ = 2.4 Hz, $^3J_{HPt}$ = 29.6 Hz), 8.17 (2H, dd, $^3J_{HH}$ = 8.8 Hz, $^4J_{HH}$ = 2.0 Hz), 7.82 (2H, d, $^3J_{HH}$ = 8.8 Hz), 7.66 (4H, d, $^3J_{HH}$ = 8.8 Hz), 7.51 (2H, d, $^3J_{HH}$ = 8.8 Hz), 7.01 (4H, d, $^3J_{HH}$ = 8.8 Hz), 6.62 (2H, dd, $^3J_{HH}$ = 8.8 Hz, $^4J_{HH}$ = 2.4 Hz), 5.64 (2H, d, $^4J_{HH}$ = 2.4 Hz, $^3J_{HPt}$ = 36.8 Hz), 4.0 (4H, t, $^3J_{HH}$ = 6.8 Hz), 3.68 (4H, m), 1.81 (4H. m), 1.47 (8H, m), 1.21 (64H, broad m), 0.87 (12H, t, $^3J_{HH}$ = 7.2 Hz); ^{195}Pt NMR (107 MHz, CDCl$_3$): δ = -1740 ppm; CHN elemental analysis: observed (calculated): %C 67.02 (67.24), %H 8.13 (8.33), %N 1.89 (1.91)

[Pt(κ^2-N^C-L)$_2$Br$_2$] (5): This was synthesised by modification of a literature procedure.[9a] To a suspension 4 (500 mg, 0.34 mmol) in acetone (150 mL) was added AgOTf (220 mg, 0.86 mmol). The mixture was stirred in the dark at reflux for 5 hours. The reaction mixture was cooled, the solvent reduced to approx. 30 ml and the solution cooled in the fridge for 16 hours. The resulting suspension was filtered through Celite®, and the filtrate concentrated *in vacuo*. The [Pt(L)$_2$OTf$_2$] intermediate was used without further purification. To this was added NaBr (1.0 g, 9.7 mmol) and the mixture heated at 50 °C for 1.5 hours in acetone (60 mL). The reaction mixture was cooled to room temperature and the solid isolated by filtration, then washed with water (50 mL) and acetone (50 mL). The solid was recrystallized from CH$_2$Cl$_2$ and hexane to give the pure product. 90 mg (17 %) ^{1}H NMR (400 MHz, CDCl$_3$): δ = 10.42 (2H, d, $^4J_{HH}$ = 2.0 Hz, $^3J_{HPt}$ = 29.6 Hz), 8.14 (2H, dd, $^3J_{HH}$ = 8.4 Hz, $^4J_{HH}$ = 1.6 Hz), 7.81 (2H, d, $^3J_{HH}$ = 8.8 Hz), 7.68 (4H, d, $^3J_{HH}$ = 8.8 Hz), 7.49 (2H, d, $^3J_{HH}$ = 8.4 Hz), 7.02 (4H, d, $^3J_{HH}$ = 8.8 Hz), 6.60 (2H, dd, $^3J_{HH}$ = 8.4 Hz, $^4J_{HH}$ = 2.0 Hz), 5.56 (2H, d, $^4J_{HH}$ = 2.0 Hz, $^3J_{HPt}$ = 36.8 Hz), 4.0 (4H, t, $^3J_{HH}$ = 6.8 Hz), 3.66 (4H, m), 1.81 (4H. m), 1.47 (8H, m), 1.21 (64H, broad m), 0.87 (12H, t, $^3J_{HH}$ = 7.2 Hz); ^{195}Pt NMR (107 MHz, CDCl$_3$): δ = -1928 ppm; CHN elemental analysis: observed (calculated): %C 63.43 (63.21), %H 7.79 (7.77), %N 1.80 (1.77)

[Pt(tolpy)$_2$Br$_2$] (6): This was synthesised by modification of a literature procedure.[9a] To a suspension 1 (68 mg, 0.11 mmol) in acetone (40 mL) was added AgOTf (72.8 mg, 0.28 mmol). The mixture was stirred in the dark at reflux for 5 hours. The reaction mixture was cooled, and the resulting suspension was filtered through Celite®, and the filtrate concentrated *in vacuo*. The [Pt(tolpy)$_2$OTf$_2$] intermediate was used without further purification. To this was added NaBr

(0.288 g, 2.8 mmol) and the mixture heated at 50 °C for 1.5 hours in acetone (35 mL). The reaction mixture was cooled to room temperature and the solid isolated by filtration, then washed with water (50 mL) and acetone (50 mL). 44 mg (57 %). ^{1}H NMR (400 MHz, CD$_2$Cl$_2$): δ = 10.09 (2H, d, $^3J_{HH}$ = 6.0 Hz, $^3J_{HPt}$ = 29.5 Hz), 8.10 (2H, td, $^3J_{HH}$ = 7.7 Hz, $^4J_{HH}$ = 1.5 Hz), 7.97 (2H, d, $^3J_{HH}$ = 8.1 Hz), 7.54 (2H, d, $^3J_{HH}$ = 8.0 Hz), 7.47 (2H, td, $^3J_{HH}$ = 6.0 Hz, $^4J_{HH}$ = 1.5 Hz), 6.97 (2H, d, $^3J_{HH}$ = 8.0 Hz), 5.79 (2H, s, $^3J_{HPt}$ = 33 Hz), 2.10 (6H, Me, s).

Acknowledgements

References

[1]   (a) S. Laschat, A. Baro, N. Steinke, F. Giesselmann, C. Hägele, G. Scalia, R. Judele, E. Kapatsina, S. Sauer, A. Schreivogel, M. Tosoni, *Angew. Chem. Int. Ed.* **2007**, *46*, 4832-4887; (b) S. Xiao, M. Myers, Q. Miao, S. Sanaur, K. Pang, M. L. Steigerwald, C. Nuckolls, *Angew. Chem. Int. Ed.* **2005**, *44*, 7390-7394; (c) J. Nelson, *Science* **2001**, *293*, 1059-1060; (d) L. Schmidt-Mende, A. Fechtenkötter, K. Müllen, E. Moons, R. H. Friend, J. D. MacKenzie, *Science* **2001**, *293*, 1119-1122; (e) S. R. Forrest, *Nature* **2004**, *428*, 911.

[2]   (a) H. Yersin, W. J. Finkenzeller, in *Highly Efficient OLEDs with Phosphorescent Materials*, Wiley-VCH Verlag GmbH & Co. KGaA, **2008**, pp. 1-97; (b) R. C. Evans, P. Douglas, C. J. Winscom, *Coord. Chem. Rev.* **2006**, *250*, 2093-2126.

[3]   (a) M. S. Lowry, S. Bernhard, *Chem. Eur. J.* **2006**, *12*, 7970-7977; (b) Y. You, S. Y. Park, *Dalton Trans.* **2009**, 1267-1282; (c) B. J. Coe, M. Helliwell, S. Sanchez, M. K. Peers, N. S. Scrutton, *Dalton Trans.* **2015**, *44*, 15420-15423; (d) R. E. Daniels, S. Culham, M. Hunter, M. C. Durrant, M. R. Probert, W. Clegg, J. A. G. Williams, V. N. Kozhevnikov, *Dalton Trans.* **2016**, *45*, 6949-6962.

[4]   (a) K. M.-C. Wong, L.-L. Hung, W. H. Lam, N. Zhu, V. W.-W. Yam, *J. Am. Chem. Soc.* **2007**, *129*, 4350-4365; (b) V. W.-W. Yam, K. M.-C. Wong, L.-L. Hung, N. Zhu, *Angew. Chem. Int. Ed.* **2005**, *44*, 3107-3110; (c) K.-C. Yim, V. K.-M. Au, L.-L. Hung, K. M.-C. Wong, V. W.-W. Yam, *Chem. Eur. J.* **2016**, *22*, 16258-16270; (d) V. K.-M. Au, D. P.-K. Tsang, Y.-C. Wong, M.-Y. Chan, V. W.-W. Yam, *J. Organomet. Chem.* **2015**, *792*, 109-116; (e) B. Y.-W. Wong, H.-L. Wong, Y.-C. Wong, M.-Y. Chan, V. W.-W. Yam, *Angew. Chem. Int. Ed.* **2017**, *56*, 302-305.

[5]   (a) A. M. Prokhorov, T. Hofbeck, R. Czerwieniec, A. F. Suleymanova, D. N. Kozhevnikov, H. Yersin, *J. Am. Chem. Soc.* **2014**, *136*, 9637-9642; (b) W. A. Tarran, G. R. Freeman, L. Murphy, A. M. Benham, R. Kataky, J. A. G. Williams, *Inorg. Chem.* **2014**, *53*, 5738-5749; (c) J. Brooks, Y. Babayan, S. Lamansky, P. I. Djurovich, I. Tsyba, R. Bau, M. E. Thompson, *Inorg. Chem.* **2002**, *41*, 3055-3066; (d) J. A. G. Williams, A. Beeby, E. S. Davies, J. A. Weinstein, C. Wilson, *Inorg. Chem.* **2003**, *42*, 8609-8611; (e) V. N. Kozhevnikov, B. Donnio, D. W. Bruce, *Angew. Chem. Int. Ed.* **2008**, *47*, 6286-6289; (f)

A. Santoro, A. M. Prokhorov, V. N. Kozhevnikov, A. C. Whitwood, B. Donnio, J. A. G. Williams, D. W. Bruce, *J. Am. Chem. Soc.* **2011**, *133*, 5248-5251; (g) V. N. Kozhevnikov, B. Donnio, B. Heinrich, J. A. G. Williams, D. W. Bruce, *J. Mater. Chem. C* **2015**, *3*, 10177-10187; (h) J. Moussa, T. Cheminel, G. R. Freeman, L.-M. Chamoreau, J. A. G. Williams, H. Amouri, *Dalton Trans.* **2014**, *43*, 8162-8165.

[6]   (a) F. Juliá, D. Bautista, P. Gonzalez-Herrero, *Chem. Commun.* **2016**, *52*, 1657-1660; (b) F. Julia, D. Bautista, J. M. Fernandez-Hernandez, P. Gonzalez-Herrero, *Chem. Sci.* **2014**, *5*, 1875-1880.

[7]   L. Chassot, A. Von Zelewsky, D. Sandrini, M. Maestri, V. Balzani, *J. Am. Chem. Soc.* **1986**, *108*, 6084-6085.

[8]   D. M. Jenkins, S. Bernhard, *Inorg. Chem.* **2010**, *49*, 11297-11308.

[9]   (a) F. Juliá, M.-D. García-Legaz, D. Bautista, P. González-Herrero, *Inorg. Chem.* **2016**, *55*, 7647-7660; (b) F. Juliá, P. González-Herrero, *Dalton Trans.* **2016**, *45*, 10599-10608.

[10]   (a) M. O'Neill, S. M. Kelly, *Adv. Mater.* **2011**, *23*, 566-584; (b) M. O'Neill, S. M. Kelly, *Adv. Mater.* **2003**, *15*, 1135-1146; (c) A. Diez, S. J. Cowling, D. W. Bruce, *Chem. Commun.* **2012**, *48*, 10298-10300; (d) Y. Wang, J. Shi, J. Chen, W. Zhu, E. Baranoff, *J. Mater. Chem. C* **2015**, *3*, 7993-8005; (e) X. Wu, G. Xie, C. P. Cabry, X. Xu, S. J. Cowling, D. W. Bruce, W. Zhu, E. Baranoff, Y. Wang, *J. Mater. Chem. C* **2018**, *6*, 3298-3309.

[11]   (a) H. Zheng, T. M. Swager, *J. Am. Chem. Soc.* **1994**, *116*, 761-762; (b) T. M. Swager, H. Zheng, *Mol. Cryst. Liq. Cryst. Sci. Technol., Sect. A* **1995**, *260*, 301-306; (c) S. T. Trzaska, H.-F. Hsu, T. M. Swager, *J. Am. Chem. Soc.* **1999**, *121*, 4518-4519; (d) L. Ziminski, J. Malthête, *J. Chem. Soc., Chem. Commun.* **1990**, 1495-1496; (e) E. Campillos, R. Deschenaux, A.-M. Levelut, R. Ziessel, *J. Chem. Soc., Dalton Trans.* **1996**, 2533-2536; (f) D. W. Bruce, X.-H. Liu, *J. Chem. Soc., Chem. Commun.* **1994**, 729-730; (g) J. P. Rourke, D. W. Bruce, T. B. Marder, *J. Chem. Soc., Dalton Trans.* **1995**, 317-318; (h) K. E. Rowe, D. W. Bruce, *J. Chem. Soc., Dalton Trans.* **1996**, 3913-3915; (i) S. Morrone, D. Guillon, D. W. Bruce, *Inorg. Chem.* **1996**, *35*, 7041-7048; (j) R. Deschenaux, B. Donnio, G. Rheinwald, F. Stauffer, G. Süss-Fink, J. Velker, *J. Chem. Soc., Dalton Trans.* **1997**, 4351-4356; (k) S. Schmidt, G. Lattermann, R. Kleppinger, J. H. Wendorff, *Liq. Cryst.* **1994**, *16*, 693-702; (l) A. M. Giroudgodquin, A. Rassat, *Comptes Rendus Acad. Sci.* **1982**, *294*, 241-243.

[12]   For a consideration of ferrocene-based liquid crystals, see: D. W. Bruce, R. Deschenaux, B. Donnio and D. Guillon, in Comprehensive Organometallic Chemistry III; Eds. R. H. Crabtree and D. M. P. Mingos, Elsevier: Oxford, UK, 2006, Vol. 12. Chapter 12.05, pp 195-294

[13]   (a) M. Ghedini, D. Pucci, G. Barberio, *Liq. Cryst.* **2000**, *27*, 1277-1283; (b) M. Ghedini, D. Pucci, A. Crispini, G. Barberio, *Organometallics* **1999**, *18*, 2116-2124.

[14]   R. J. Allenbaugh, C. K. Schauer, A. Josey, J. D. Martin, D. V. Anokhin, D. A. Ivanov, *Chem. Mater.* **2012**, *24*, 4517-4530.

[15]   (a) E. I. Szerb, A. M. Talarico, I. Aiello, A. Crispini, N. Godbert, D. Pucci, T. Pugliese, M. Ghedini, *Eur. J. Inorg. Chem.* **2010**, *2010*, 3270-3277; (b) A. M. Prokhorov, A. Santoro, J. A. G. Williams, D. W. Bruce, *Angew. Chem. Int. Ed.* **2012**, *51*, 95-98.

[16]   (a) E. A. Katlenok, K. P. Balashev, *Russ. J. Gen. Chem.* **2013**, *83*, 2113-2114; (b) C. P. Newman, K. Casey-Green, G. J. Clarkson, G. W. V. Cave, W. Errington, J. P. Rourke, *Dalton Trans.* **2007**, 3170-3182.

[17]   A. Santoro, M. Wegrzyn, A. C. Whitwood, B. Donnio, D. W. Bruce, *J. Am. Chem. Soc.* **2010**, *132*, 10689-10691.

[18]   A. Santoro, A. C. Whitwood, J. A. G. Williams, V. N. Kozhevnikov, D. W. Bruce, *Chem. Mater.* **2009**, *21*, 3871-3882.

[19]   S. R. Whitfield, M. S. Sanford, *Organometallics* **2008**, *27*, 1683-1689.

[20]   (a) S. Fernández, J. Forniés, B. Gil, J. Gómez, E. Lalinde, *Dalton Trans.* **2003**, 822-830; (b) N. M. Shavaleev, H. Adams, J. Best, R. Edge, S. Navaratnam, J. A. Weinstein, *Inorg. Chem.* **2006**, *45*, 9410-9415; (c) P. I. Djurovich, D. Murphy, M. E. Thompson, B. Hernandez, R. Gao, P. L. Hunt, M. Selke, *Dalton Trans.* **2007**, 3763-3770; (d) P.-H. Lanoë, J.-L. Fillaut, L. Toupet, J. A. G. Williams, H. L. Bozec, V. Guerchais, *Chem. Commun.* **2008**, 4333-4335; (e) F. Niedermair, O. Kwon, K. Zojer, S. Kappaun, G. Trimmel, K. Mereiter, C. Slugovc, *Dalton Trans.* **2008**, 4006-4014; (f) D. L. Rochester, S. Develay,

S. Záliš, J. A. G. Williams, *Dalton Trans.* **2009**, 1728-1741; (g) J. Forniés, S. Fuertes, A. Martín, V. Sicilia, B. Gil, E. Lalinde, *Dalton Trans.* **2009**, 2224-2234; (h) J. R. Berenguer, Á. Díez, A. García, E. Lalinde, M. T. Moreno, S. Sánchez, J. Torroba, *Organometallics* **2011**, *30,* 1646-1657; (i) A. Colombo, C. Dragonetti, D. Marinotto, S. Righetto, D. Roberto, S. Tavazzi, M. Escadeillas, V. Guerchais, H. Le Bozec, A. Boucekkine, C. Latouche, *Organometallics* **2013**, *32,* 3890-3894; (j) J. Moussa, G. R. Freeman, J. A. G. Williams, L.-M. Chamoreau, P. Herson, H. Amouri, *Eur. J. Inorg. Chem.* **2016**, *2016,* 761-767; (k) T. Zou, C.-N. Lok, Y. M. E. Fung, C.-M. Che, *Chem. Commun.* **2013**, *49,* 5423-5425; (l) H. Uesugi, T. Tsukuda, K. Takao, T. Tsubomura, *Dalton Trans.* **2013**, *42*, 7396-7403.

[21]   M. M. Mdleleni, J. S. Bridgewater, R. J. Watts, P. C. Ford, *Inorg. Chem.* **1995**, *34*, 2334-2342.

[22]   D. N. Kozhevnikov, V. N. Kozhevnikov, M. Z. Shafikov, A. M. Prokhorov, D. W. Bruce, J. A. Gareth Williams, *Inorg. Chem.* **2011**, *50*, 3804-3815.

[23]   (a) M. Cocchi, J. Kalinowski, V. Fattori, J. A. G. Williams, L. Murphy, *Appl. Phys. Lett.* **2009**, *94*, 073309; (b) J. Kalinowski, M. Cocchi, L. Murphy, J. A. G. Williams, V. Fattori, *Chem. Phys.* **2010**, *378*, 47-57.

[24]   M. Spencer, A. Santoro, G. R. Freeman, A. Diez, P. R. Murray, J. Torroba, A. C. Whitwood, L. J. Yellowlees, J. A. G. Williams, D. W. Bruce, *Dalton Trans.* **2012**, *41*, 14244-14256.

[25]   K. Nakamaru, *Bull. Chem. Soc. Jpn.* **1982**, *55*, 2697-2705.

[26]   CrysAlisPro, Oxford Diffraction Ltd. Version 1.171.34.41

[27]   Empirical absorption correction using spherical harmonics, implemented in SCALE3 ABSPACK scaling algorithm within CrysAlisPro software, Oxford Diffraction Ltd. Version 1.171.34.40

[28]   O. V. Dolomanov, L. J. Bourhis, R. J. Gildea, J. A. K. Howard, H. Puschmann, *J. Appl. Crystallogr.* **2009**, *42*, 339-341.

[29]   SUPERFLIP - a computer program for the solution of crystal structures by charge flipping in arbitrary dimensions, L. Palatinus, G. Chapuis, *J. Appl. Crystallogr.* **2007**, *40*, 786-790.

[30]   SHELXT – Integrated space-group and crystal-structure determination, G. Sheldrick, *Acta Crystallogr. A* **2015**, *71*, 3-8.

[31]   SHELXL-97- Program for the Refinement of Crystal Structures. G. Sheldrick, *Acta Crystallogr. A* **2008**, *64*, 112-122.

[32]   (a) P. Császár, P. Pulay, *J. Mol. Struct.* **1984**, *114*, 31-34; (b) R. Ahlrichs, M. Bär, M. Häser, H. Horn, C. Kölmel, *Chem. Phys. Lett.* **1989**, *162*, 165-169; (c) P. Deglmann, F. Furche, R. Ahlrichs, *Chem. Phys. Lett.* **2002**, *362*, 511-518; (d) P. Deglmann, K. May, F. Furche, R. Ahlrichs, *Chem. Phys. Lett.* **2004**, *384*, 103-107; (e) K. Eichkorn, O. Treutler, H. Öhm, M. Häser, R. Ahlrichs, *Chem. Phys. Lett.* **1995**, *242*, 652-660; (f) K. Eichkorn, F. Weigend, O. Treutler, R. Ahlrichs, *Theor. Chem. Acc.* **1997**, *97*, 119-124; (g) O. Treutler, R. Ahlrichs, *J. Chem. Phys.* **1995**, *102*, 346-354; (h) M. von Arnim, R. Ahlrichs, *J. Chem. Phys.* **1999**, *111*, 9183-9190.